Molecular Catalysis 479 (2019) 110629

Contents lists available at ScienceDirect

Molecular Catalysis

journal homepage: www.elsevier.com/locate/mcat

Synthesis and characterization of tridentate phosphine ligands incorporating long methylene chains and ethoxysilane groups for immobilizing molecular rhodium catalysts

J. Guenther, J. Reibenspies, J. Blümel*

Texas A&M University, Department of Chemistry, P.O. Box 30012, College Station, TX, 77842-3012, USA

ARTICLE INFO

Keywords:
Immobilized catalysts
Phosphine linkers
Ethoxysilanes
HRMAS NMR
Olefin hydrogenation
rhodium catalysts

ABSTRACT

The new tridentate phosphine ligands $EtOSi((CH_2)_nPPh_2)_3$ and $O[Si((CH_2)_nPPh_2)_3]_2$ (n = 4, 7, 11), as well as their precursor ethoxysilanes $EtOSi((CH_2)_mCH = CH_2)_3$ and disiloxanes $O[Si((CH_2)_mCH = CH_2)_3]_2$ (m = 2, 5, 9) and $EtOSi((CH_2)_{11}PPh_2RhClCOD)_3$ (COD = cyclooctadiene) have been synthesized and fully characterized. The ethoxysilane- and disiloxane-containing phosphine ligands have been immobilized on silica *via* covalent siloxane bonds. The immobilized linkers have been characterized by ^{31}P and ^{29}Si CP/MAS and HRMAS NMR spectroscopy. The covalent siloxane bonds between the linkers and the silica surface prevent translational mobility of the phosphines. Immobilized Wilkinson-type Rh hydrogenation catalysts have been obtained by ligand exchange of $ClRh(PPh_3)_3$ and ClRhpyCOD (py = pyridine) with the surface-bound ligands. The single crystal X-ray structure of ClRhpyCOD has been reported. The activities and lifetimes have been studied for the hydrogenation of 1-dodecene. The new catalysts are highly active and they can be recycled up to 15 times without major loss of activity. Within the first hours of the catalytic reaction the initially molecular complexes form Rh nanoparticles with a narrow size distribution on the surface. The nanoparticles do not leach into the supernatant solution and are not air-sensitive.

Introduction

Catalysis represents one of the most central aspects of synthetic chemistry in academia and industry. However, the "ideal catalyst" [1] featuring superior activity, total selectivity and eternal lifetime, has not yet been discovered. On the way there, diverse approaches have been studied to facilitate the removal and recyclability of highly active, originally homogeneous catalysts. One successful approach makes use of a biphasic liquid system, with one fluorous and one conventional organic phase, by controlling their miscibility *via* temperature [2]. In another approach a Rh catalyst was adsorbed on a teflon tape and reversibly released into solution as a homogeneous catalyst [3].

Catalysts immobilized on oxide supports, in particular, are of enormous interest because they can be recovered and reused, while remaining as active and reactive as their homogeneous analogs. In contrast to common belief, immobilized catalysts already play a major role in fine chemicals production [4]. Optimally, an immobilized catalyst retains all the superior qualities of the homogeneous analog, while it allows for easy catalyst separation from the reaction mixture, batchwise recycling, or application in a continuous flow setting [4].

Our group has successfully pursued the immobilization of catalysts on solid supports *via* diverse monophosphine [5–8] and chelating diphosphine linkers [5,9–11]. The most conventional way to achieve the covalent tethering of linkers to oxide support surfaces is *via* intramolecular ethoxysilane groups. In order to exclude any leaching of the linker and therewith detachment of the whole catalyst from the support surface, the reactions of mono- and triethoxysilanes with oxide surfaces have been studied in detail [6,12,13].

While more exotic solid supports like zirconium phosphate nanoplatelets [14] and various other oxides have been employed as support [6], silica [15,16] remains the most favorable support for immobilized catalysts. Silica is inexpensive and available from suppliers in a large variety of particle and pore sizes. Most importantly, it is mechanically robust, stable at higher temperatures, and settles within minutes after the reaction. The supernatant containing the products can simply be decanted, and there is no need for filtration or centrifugation. After washing the silica, the covalently bound immobilized catalyst can be used for the next catalytic run.

Bifunctional phosphine linkers incorporating ethoxysilane groups have been applied to immobilize Ni catalysts for the cyclotrimerization

* Corresponding author.
E-mail address: bluemel@tamu.edu (J. Blümel).

https://doi.org/10.1016/j.mcat.2019.110629
Received 2 August 2019; Received in revised form 10 September 2019; Accepted 12 September 2019
Available online 24 September 2019
2468-8231/

of acetylenes [17–19], Pd/Cu catalyst systems for Sonogashira reactions [20–22], and Rh catalysts for olefin hydrogenation [23–25]. All catalysts displayed unprecedented activities and could be recycled many times.

Nevertheless, some problems remain. For example, neighboring catalyst molecules on the surface can dimerize or agglomerate. Wilkinson's catalyst has a tendency to dimerize already at room temperature, and the dimer is no longer catalytically active [26]. Accordingly, it has been determined that diluting immobilized Wilkinson-type catalysts on the surface improves their performance substantially [24]. However, this approach increases the bulk of the support, a scenario which is very unpopular in industrial settings.

Another problem arises when linkers decompose due to reactions with the silica surface [27]. Additionally, phosphine linkers incoporating ethoxysilane groups can be transformed into the corresponding ethylphosphonium salts by reacting with the silica surface at high temperatures [28]. These P(V) species can no longer coordinate metal complexes. To avoid any reactions of the phosphines and metal centers with the reactive silica surface, we have explored rigid tetraphosphine linker systems with tetraphenyl- and tetrabiphenyl element cores [29–31]. These rigid linkers prevented Rh catalysts from dimerizing and kept the metal centers from interacting with the surface [31]. However, the monodentate phosphines did not entirely prevent the metal centers from eventually getting detached and forming nanoparticles in the case of Wilkinson-type Rh catalysts [31].

The detachment of a metal complex from monodentate linkers ("leaching") leads to the gradual loss of metal complexes upon recycling of the catalyst and potentially nanoparticle formation. Over the years we have investigated this important issue using diverse immobilized catalysts. For example, it has been demonstrated with classical ^{31}P CP/MAS (cross-polarization with Magic Angle Spinning) solid-state NMR [32,33] that the gradual oxidation of the phosphine linkers leads to the loss of the metal centers because phosphine oxides cannot coordinate them any longer [28]. Unfortunately, CP/MAS of dry materials only allows the measurements before and after catalysis. The HRMAS (high-resolution MAS) method [20–23,27,34], however, gives real time insight of the processes taking place in the presence of a solvent [20–22]. This straightforward technique has been used recently to monitor the *in situ* migration of $PdCl_2$ fragments over the "lawn of linkers" on silica surfaces [20–22]. Furthermore, it allowed the ranking of phosphine linkers with respect to their abilities to retain the Pd centers [20]. These studies confirmed that chelating phosphine linkers are best suited to firmly coordinate to metal centers [20]. Catalysis results with different Ni complexes coordinated by chelating tripodal phosphine ligands corroborated this conclusion [19].

Olefin hydrogenation is one of the most studied catalytic reactions [35]. Selected immobilized monodentate and chelating phosphine linkers and Wilkinson-type Rh complexes thereof have already been tested for their activity and recyclability with respect to the important catalytic olefin hydrogenation [14,23–25,30,31]. Therefore, there is already a substantial body of data on Rh-catalyzed hydrogenation under standardized conditions from our group [14,23–25,30,31]. A comparison with the hydrogenation results of other groups, obtained with different biphasic catalytic systems, should be interesting as well [36].

In particular, we described the immobilization of tridentate phosphine linkers incorporating long methylene chains using electrostatic interactions of the surface with an intramolecular phosphonium group (Fig. 1, right) [23]. The long tethers have the advantage of providing maximal mobility to the metal complexes in the presence of a solvent, in this way mimicking a homogeneous catalyst. This mobility is also advantageous for ^{31}P HRMAS NMR analysis because it leads to minimal signal halfwidths [20–23,27,34]. No ligand leaching was observed in non-polar solvents, such as toluene, and highly active hydrogenation catalysts were obtained after coordination of Rh to the immobilized phosphine ligands [23]. However, it turned out that the molecular mononuclear species decomposed rather quickly to form Rh

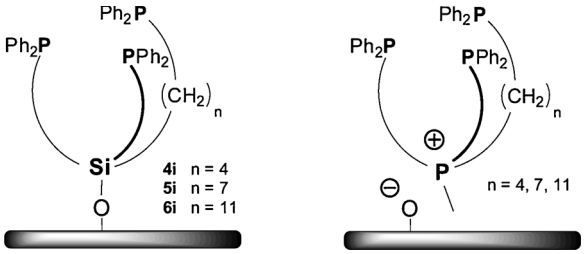

Fig. 1. Tridentate phosphine linkers incorporating ethoxysilane and phosphonium groups [23] for immobilizing Rh catalysts on silica *via* covalent bonds and electrostatic interactions.

nanoparticles with a narrow size distribution on the surface [23]. The nanoparticles themselves constituted an active hydrogenation catalyst, but the controlled ligand environment of a molecular species was lost. NMR experiments suggest that, although the phosphonium linkers do not leach off the surface, they are translationally mobile on the surface, which is suspected to facilitate the formation of Rh nanoparticles [37]. The metal centers could, for example, be delivered directly and deposited on nanoparticles on the surface by the mobile linkers. Furthermore, the influence of the phosphonium group itself on the formation of the nanoparticles and the timeline of the nanoparticle formation are still unknown.

The main goal of the present work is to test whether the linker mobility on the surface and the phosphonium group of the previously described system (Fig. 1, right) have an influence on the Rh nanoparticle formation of immobilized Wilkinson-type catalysts. Specifically, we sought to improve the catalyst performance by immobilizing similar tridentate phosphine linkers on silica in a covalent manner *via* ethoxysilanes (Fig. 1, left). The covalent attachment renders translational mobility impossible. For this purpose, the ligands **4**, **5**, and **6** were synthesized and immobilized on silica (Scheme 1). The immobilized ligands and the respective Rh complexes were characterized by solid-state NMR. The catalysts' activities for the hydrogenation of 1-dodecene and their lifetimes were studied. Furthermore, the nature of the active species, especially with respect to nanoparticle formation,

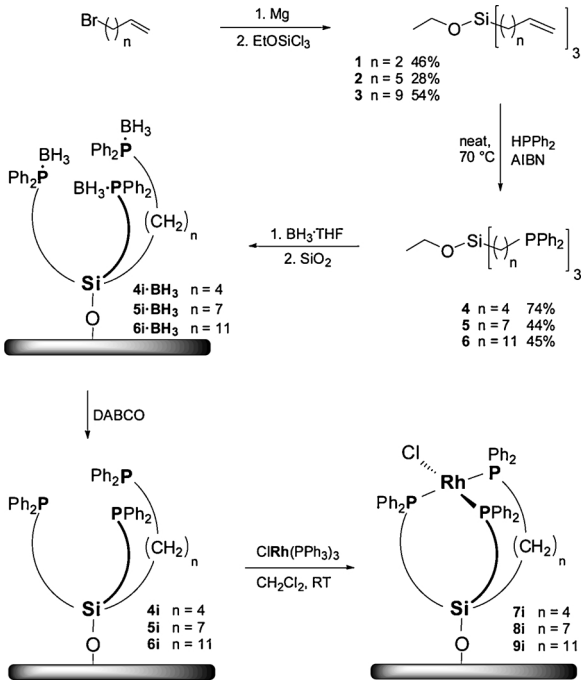

Scheme 1. Synthesis of the phosphine ligands **4**, **5**, and **6**, their immobilization on SiO_2, and formation of the immobilized Rh complexes **7i**, **8i**, and **9i**.

was investigated. In the following we present key results in our ongoing systematic study of immobilized Rh catalysts.

Results and discussion

Synthesis of the phosphine linkers

The phosphine ligands **4-6** were synthesized in good yields in two steps from the respective bromoalkenes $Br(CH_2)_nCH = CH_2$ (n = 2, 5, 9) [8]. The bromoalkenes were subsequently treated with Mg to form the Grignard reagents and coupled *in situ* with $EtOSiCl_3$ to give **1-3** as clean, colorless liquids. Condensation of the ethoxysilane moieties led to the partial formation of the disiloxanes $O[Si((CH_2)_nCH = CH_2)_3]_2$ (n = 2, 5, 9) (**1d-3d**). The latter could be separated from **1-3** by column chromatography, isolated, and characterized. The ethoxysilane linkers **4-6** were obtained by hydrophosphination of **1-3** with a slight excess of Ph_2PH in the presence of AIBN as a radical starter as described by Stelzer [38]. The hexaphosphines incorporating a disiloxane group $O[Si((CH_2)_nPPh_2)_3]_2$ (n = 4, 7, 11) (**4d-6d**) were synthesized in the same way by hydrophosphination of **1d-3d**.

After the sraightforward synthesis, all molecular ethoxysilanes were obtained with sufficient purity (< 1% trace impurities, see Supplementary Material) to proceed to the immobilization on silica.

Immobilization of the phosphine linkers

The most conventional way to immobilize phosphine linkers on oxide supports is by using intramolecular ethoxysilane groups. The reactions of ethoxysilanes with silica have been studied earlier. The mechanism can consist of an addition of the ethoxysilane function to surface siloxane groups. This is the preferred pathway when using dried silica [12a]. In this way, most of the ethoxy groups remain bound to the surface at the neighboring sites [12a]. Alternatively, the ethoxysilane group is first hydrolyzed and subsequently a condensation reaction with surface silanol groups to form the covalent Si—O—Si bond takes place [12a]. Most importantly, during the immobilization step non polar and non protic solvents such as hexanes, or toluene should be applied. Polar solvents are strongly adsorbed on the surface and prevent the ethoxysilane from contact. For example, it has been found that in case diglyme was used as the solvent, even at very high temperatures no ethoxysilane was found covalently bound on the surface after prolonged reaction times [12b].

Typically, phosphine linkers for immobilizations incorporate $Si(OEt)_3$ groups [5], which can be anchored to oxide surfaces at low temperatures. However, due to their tripodal nature, linkers **4-6** (Scheme 1) only contain one OEt group. Therefore, higher temperatures of 60–70 °C were required to achieve appreciable surface loadings and create covalent Si—O—Si bonds [Table 1]. Earlier work has revealed that the temperature should not be too high, though, because the amount of quaternized phosphonium salts increases with temperature [28]. Another issue arises from the easy oxidation of the alkylphosphines to the phosphine oxides. The sample in the first entry in Table 1, for example, showed traces of phosphine oxides [39,40] and phosphonium salts [28] after direct immobilization of **4**. Both, phosphonium salts and phosphine oxides are no longer able to coordinate to metal centers and just block surface sites. Fortunately, both can be prevented by protecting the linkers by *in situ* reaction of **4-6** with $THF{\cdot}BH_3$ prior to the immobilization step (Scheme 1). The obtained protected linkers could then be immobilized at elevated temperatures on silica as **4i·BH$_3$-6i·BH$_3$**. After the immobilization step the phosphines were deprotected with DABCO (1,4-diazabicyclo[2.2.2]octane) at ambient temperature to yield **4i-6i**.

Table 1
Surface coverages of the modified silica **4i-6i** and **4di-6di** with the corresponding molecular ethoxysilanes **4-6** and disiloxanes **4d-6d**. The ligands were protected prior to immobilization at the indicated temperature in toluene.

Material	T [°C]	Molecules per 100 nm^2 SiO_2	mmol of linker per g of SiO_2
4i[a]	70	11.5[a]	0.143[a]
4i	70	8.2	0.110
4i	60	3.2	0.040
4di	90	14.6	0.183
5i	70	3.0	0.037
5di	70	5.4	0.068
6i	80	2.7	0.034
6di	90	10.2	0.127

[a] SiO_2 and unprotected ligand **4** were stirred in toluene overnight at 70 °C, and traces of oxides and phosphonium salt were found in **4i**.

As an alternative to the ethoxysilanes **4-6** the immobilization could also be carried out with the corresponding disiloxanes $O[Si((CH_2)_{4,7,11}PPh_2)_3]_2$ (**4d-6d**). Higher temperatures were applied to make sure that chemical reactions with the silica surface and covalent bonding occurred. Consequently, the loadings of **4di-6di** were slightly higher than those obtained with the ethoxysilanes **4i-6i**. Interestingly, comparing **5i** with **5di**, obtained at the same reaction temperature, the loading with the disiloxane **5d** was higher. This might indicate that the molecular preorganization of two linkers in close proximity allows for a more dense surface coverage. For all linker immobilizations, the reaction temperatures and the corresponding surface coverages are summarized in Table 1.

Importantly, apart from the "pairing" of the linkers for **4di-6di**, the applied immobilization methodology leads to highly dispersed linkers **4i-6i** on the silica surface when using the comparatively low loadings (Table 1) [24b]. Using triethoxysilanes it was observed that the reaction conditions influenced the distribution on the surface. Condensation of the precursors in solution prevents highly dispersed ligand sites on the support. Monoethoxysilanes like **4-6** prevent any further condensation and clustering of the linkers on the surface.

Solid-state NMR of immobilized phosphines

The silica materials functionalized with phosphine ligands **4i-6i** and **4di-6di** were characterized by multinuclear solid-state NMR spectroscopy. State-of-the-art ^{29}Si CP/MAS, ^{31}P CP/MAS [32,33], and ^{31}P HRMAS NMR techniques were applied [20–23,27,34]. The ^{29}Si CP/MAS spectra are valuable tools to prove the covalent bonding of the linkers to the silica surface [12]. Covalently bound silanes exhibit a broad resonance of low intensity, while mobile, merely adsorbed silanes would emerge as a narrow line [8]. The signals of covalently bound triethoxysilanes and ethoxysilanes have already been described previously [12b,13]. With the present set of linkers it was especially important to prove the covalent bonding of the disiloxanes **4di-6di** on the surface. For example, the ^{29}Si CP/MAS spectrum of immobilized **4di** shows a broad signal with low intensity at 4.5 ppm (Fig. 2). This chemical shift is characteristic for ethoxysilanes covalently bound to a silica surface [13]. The resonance at -104 corresponds to the ^{29}Si nuclei at the binding site on the surface, overlapping with the signal of surface silanol groups. The ^{29}Si signal at about -110 stems from the bulk Si nuclei [12b,13,32b].

In the ^{31}P CP/MAS NMR spectra, the immobilized borane-protected phosphines **4i·BH$_3$-6i·BH$_3$** lead to resonances at about 20 ppm, which lies within the chemical shift range that is characteristic for borane adducts of phosphines [21]. One example, the ^{31}P CP/MAS spectrum of **6i·BH$_3$** is displayed in Fig. 3 (top). The deprotection of the surface-bound **6i·BH$_3$** by adding an excess of DABCO to a slurry of the silica in a solvent is quantitative. The peak at 20 ppm disappears and a new signal, shifted upfield to around -16 ppm, appears, corresponding to the deprotected immobilized phosphine **6i** (Fig. 3, middle). This result is important with respect to the catalytic reactions performed with a Rh complex bound to the linker, as described below. It shows that substrates can easily diffuse into the pores of the support material and

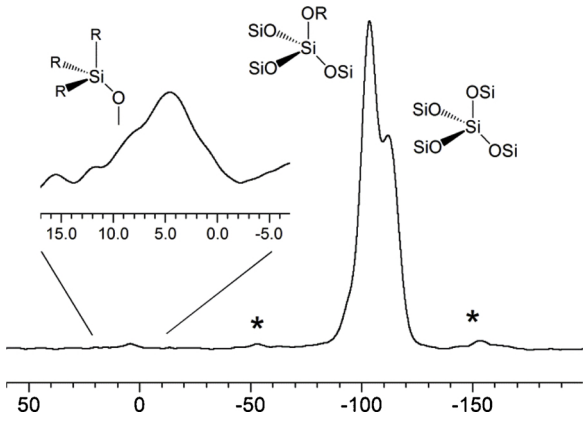

Fig. 2. ^{29}Si CP/MAS NMR of **4di** recorded with a spinning frequency of ν_{rot} = 4 kHz. Asterisks denote rotational sidebands of the signal at −104 ppm.

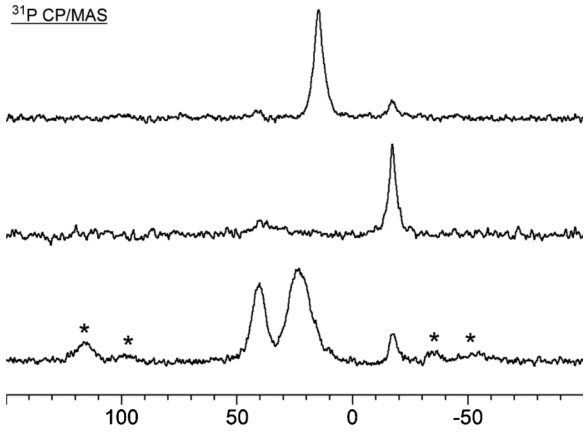

Fig. 3. ^{31}P CP/MAS NMR of **6i**·BH_3 (top), **6i** (middle) and **9i** (bottom) with ν_{rot} = 10 kHz. Asterisks denote spinning sidebands.

reach all catalytically active sites.

When a Wilkinson-type Rh complex is coordinated by the surface-tethered linker **6i**, new ^{31}P CP/MAS signals for the catalyst **9i** emerge at 23 and 40 ppm (Fig. 3, bottom) [24,25]. Only a trace of uncoordinated phosphine remains.

The long alkyl chains of the tethered linkers lead to increased mobilities of the phosphine moieties in the presence of an organic solvent. As described earlier for linkers incorporating long methylene chains [23], this mobility, in combination with magic angle spinning (MAS) makes the functionalized silica materials **4i**-**6i** amenable to characterization by ^{31}P HRMAS NMR [20–23,27,34]. The linewidth in HRMAS NMR qualitatively reflects the mobility of immobilized species because the motion leads to partial averaging of the main anisotropic interactions in the solid state, the chemical shift anisotropy (CSA) and dipolar interactions [32,33]. Initial HRMAS measurements were carried out in toluene. Following expectations, the halfwidths of the signals drastically decrease, compared to the linewidth of the resonances obtained by ^{31}P CPMAS of the dry materials (Fig. 4). This is advantageous because the measurement times are much shorter, minutes with HRMAS *versus* hours for the dry modified silica. More importantly, the spectral resolution is improved substantially due to the diminished signal halfwidths. For example, for **6i** the signal halfwidth decreases from 559 Hz to 93 Hz when a small amount of toluene is added to the dry sample to increase the mobility of the linker (Fig. 4). Importantly, during HRMAS the phosphine linker is not detached from its binding site and translationally mobile on the surface, as it is the case for merely surface-adsorbed species [39f,39g,41]. Furthermore, the linker is not leached into solution as the much larger linewidth of 93 Hz for **6i** as compared with

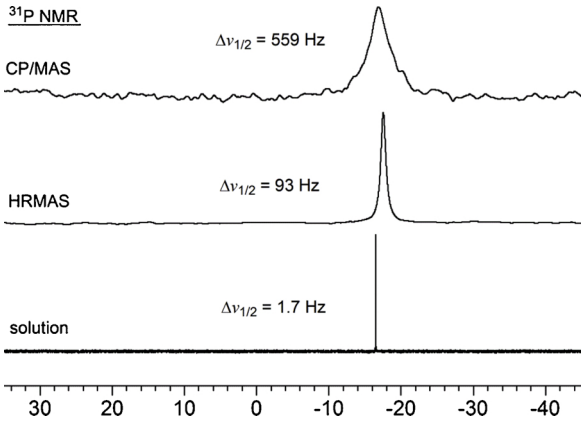

Fig. 4. ^{31}P NMR spectrum of **6** ($CDCl_3$, bottom), ^{31}P HRMAS of a slurry of **6i** in toluene (middle, ν_{rot} = 2 kHz), and ^{31}P CP/MAS spectrum of dry **6i** (top, ν_{rot} = 10 kHz).

Table 2
$\delta(^{31}P)$ from MAS and HRMAS spectra and signal halfwidths $\Delta\nu_{1/2}$ of the immobilized phosphines **4i**-**6i**. Spinning speeds: 10 kHz for MAS and 2 kHz for HRMAS (toluene).

Immobilized Phosphine	$\delta(^{31}P)$ [ppm]		$\Delta\nu_{1/2}$ [Hz]	
	MAS	HRMAS	MAS	HRMAS
4i	−16.78	−16.84	1351	480
5i	−17.16	−17.50	900	130
6i	−16.87	−17.53	559	93

the halfwidth of the resonance of **6** in chloroform solution (1.7 Hz) proves (Fig. 4).

Table 2 summarizes the chemical shifts and signal halfwidths of **4i**-**6i** for MAS of the dry materials and HRMAS measurements in the presence of toluene. According to intuition, the linewidth decreases with increasing mobility and with the alkyl chain length, from 480 Hz for **4i**, over 130 Hz for **5i**, to 93 Hz for **6i**. The ^{31}P chemical shifts obtained by MAS of the dry materials *versus* HRMAS of **4i**-**6i** in toluene do not undergo changes larger than about 0.6 ppm upfield (Table 2). These chemical shift changes do not exceed the typical variations of $\delta(^{31}P)$ when different solvents, or none at all, are used for NMR measurements.

^{31}P HRMAS spectra for **6i** were recorded in various common organic solvents relevant for synthesis and catalysis (Table 3). Since the solubility of **6** with the long methylene chain is equally high in protic and non protic solvents, and the polarity does not play a big role, the halfwidths of the HRMAS signals of **6i** is for many solvents within the narrow range of 83–93 Hz. Only the least polar solvent hexane and acetone lead to somewhat broader lines of up to 205 Hz.

One of the main goals of this study was to compare the mobilities and catalytic activities of Rh complexes immobilized by electrostatic interactions of phosphonium salt functions in the linkers with those complexes tethered *via* covalently bound ethoxysilane linkers.

Table 3
^{31}P HRMAS signal halfwidths $\Delta\ \nu_{1/2}$ of **6i** and **10i** in the indicated solvents.

Solvent	**6i** $\Delta\nu_{1/2}$ [Hz]	**10i** $\Delta\nu_{1/2}$ [Hz]
MeOH	83	24
MeCN	83	22
THF	90	34
Acetone	142	34
CH_2Cl_2	90	20
Toluene	93	26
Hexane	205	134

Therefore, we sought to compare the mobilities of **6i** with those of a linker with the same number of methylene groups, $(CH_2)_{11}$, but being bound to the surface by a phosphonium iodide group, with HRMAS. The linker **10i**, derived from immobilization of the phosphonium salt $[CH_3P((CH_2)_{11}PPh_2)_3]^+ I^-$ (**10**) [23] on silica, was chosen for the comparison. The halfwidths of the ^{31}P HRMAS signals of **6i** and **10i** in various solvents are summarized in Table 3. In the presence of all solvents the lines are substantially broader in the case of the covalently bound phosphine **6i**. Since the alkyl chain length is the same in both linkers, the mobilities of the phosphine-carrying "arms" should be comparable. This means that for **10i** an additional mode of mobility must be present. Since **10i** is not detached from the surface by the solvents [23], the mobility can only consist of translational motion of **10i** across the surface within the pores. For catalysts immobilized *via* linkers such as **10i**, nanoparticle formation occurred during hydrogenation, potentially aided by the translational mobility of the linkers [23]. The HRMAS measurements of both linker types show that the ligands **4i**-**6i** still retain a high degree of mobility, but they are fixed at one specific surface site. Therefore, the coordinated metal complexes should mimic homogeneous catalysts, while their covalent attachment to the surface should prevent clustering and nanoparticle formation as a potential pathway of catalyst decomposition.

Immobilization of the rhodium catalysts

The immobilized Rh complexes **7i**-**9i** have been obtained from **4i**-**6i** by ligand exchange with Wilkinson's catalyst $RhCl(PPh_3)_3$ at room temperature (Scheme 1) [24,25]. ^{31}P CP/MAS NMR shows that none of the liberated PPh_3 remains adsorbed on the surface after washing the material with toluene (Fig. 3, bottom). The phosphine coordinated *trans* to the Cl ligand leads to a peak at 40.29 ppm and the two phosphines in *cis* position are found at 24.04 ppm [24,25].

Additionally, soluble Rh precursors for the immobilization that lack PPh_3 ligands are of interest because the immobilization of Wilkinson's catalyst can lead to the formation of the dimeric complex $[(PPh_3)_2RhCl]_2$ at elevated temperatures, which is strongly adsorbed on the silica surface [26]. It is also not catalytically active for olefin hydrogenation [26a]. Therefore, ClRhpyCOD (py = pyridine, COD = cyclooctadiene) (**11**) has been investigated as an alternative metal complex precursor for the immobilization *via* ligand exchange.

Although the complex was published as early as 1973 [42], its crystal structure has not yet been reported. Crystals suitable for single crystal X-ray diffraction were obtained by slow evaporation of the solvent from a solution of **11** in MeCN [43]. The structure shows a square planar geometry with respect to the coordinating atoms N and Cl and the centers of the C=C bonds (Fig. 5) [43]. All bond lengths and

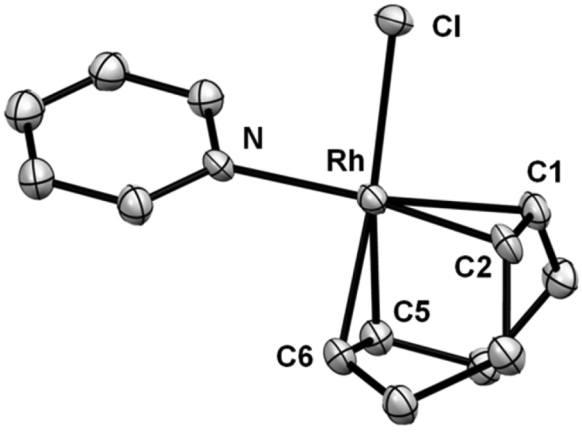

Fig. 5. Single crystal X-ray structure of ClRhpyCOD (**11**) showing 50% thermal ellipsoid probability of one of the two independent molecules. H atoms are omitted for clarity [43].

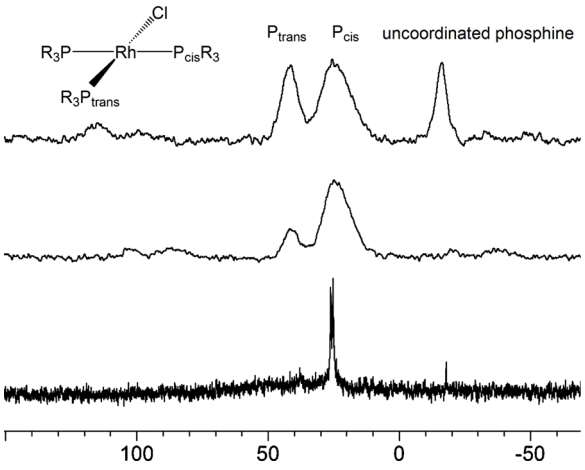

Fig. 6. ^{31}P CP/MAS NMR spectra after the reaction of **6i** with one equivalent (top) and three equivalents (middle) of RhClpyCOD (**11**). Bottom: ^{31}P HRMAS spectrum (slurry in acetone) of **6i** after reaction with three equivalents of **11**.

Table 4
Selected bond lengths (Å) and angles (°) of ClRhpyCOD (**11**) [43].

Bond lengths [Å]		Bond angles [°]	
Rh – N	2.118(3) / 2.105(3)	N – Rh – Cl	87.85(9) / 89.38(9)
Rh – Cl	2.3755(11) / 2.3914(10)	N – Rh – C2	158.30(14) / 160.42(14)
Rh – C1	2.158(4) / 2.127(4)	N – Rh – C1	163.66(13) / 161.52(14)
Rh – C2	2.134(4) / 2.130(4)	C6 – Rh – N	91.75(13) / 90.72(14)
Rh – C5	2.112(4) / 2.111(4)	C5 – Rh – N	93.83(13) / 91.96(14)
Rh – C6	2.113(4) / 2.111(4)	Cl – Rh – C5	157.76(10) / 158.85(13)
C1 – C2	1.399(5) / 1.388(6)	Cl – Rh – C6	163.36(11) / 162.63(13)
C5 – C6	1.406(5) / 1.391(7)		

angles are in the expected range. Selected data are summarized in Table 4. Rajput et al. reported the X-ray structure of a related square planar complex incorporating a ferrocenyl-substituented pyridine ligand [44]. In this compound, for example, the Rh—Cl distance amounts to 2.358 Å, a value close to the 2.3755(11)/2.3914(10) Å found in **11**. The bonds to the C atoms *trans* to pyridine are lengthened as compared to the Rh—C bonds *trans* to Cl [44]. For **11**, the distances Rh—C1 and Rh—C2 are also longer (2.158(4)/2.127(4) Å and 2.134(4)/2.130(4) Å) than those for Rh—C5 and Rh—C6 (2.112(4)/2.111(4) Å and 2.113(4)/2.111(4) Å). The complex reported by Rajput et al. also displays a N—Rh—Cl bond angle of 88.26° [44], which is comparable to the value in **11** (87.85(9)°/89.38(9)°) (Table 4).

The ligand exchange reactions were carried out using **4i**-**6i** and **11** to yield **12i**-**14i** in analogy to the procedure described for Wilkinson's catalyst (Scheme 2). It is noteworthy that the materials obtained after thorough washing were yellow or slightly orange as compared to the bright orange silica obtained when using $ClRh(PPh_3)_3$ for the ligand exchange. This is a first indication that **12i**-**14i** are not identical to **7i**-**9i**.

The functionalized materials **12i**-**14i** were also analyzed by ^{31}P CP/MAS and ^{31}P HRMAS NMR (Figs. 6 and 7). When reacting **6i** with one equivalent of RhClpyCOD (**11**) per tripodal linker, a spectrum similar to that of **9i** is observed (Fig. 6, top). However, it shows a large signal corresponding to uncoordinated, albeit surface-bound phosphine. When using three equivalents of **11** no uncoordinated phosphine remains and the intensity of the peak at 25 ppm, which corresponds to a phosphine

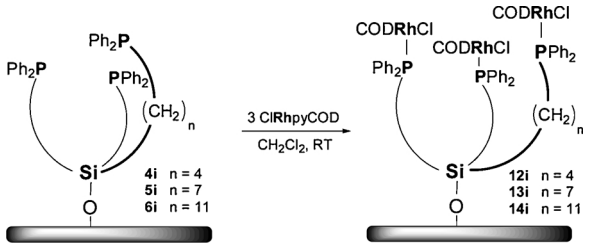

Scheme 2. Synthesis of the immobilized Rh complexess **12i**, **13i**, and **14i**.

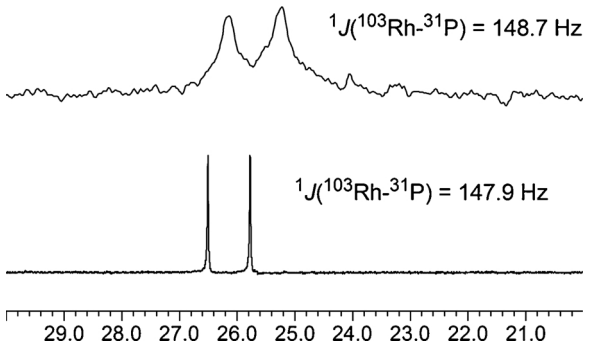

Fig. 7. ^{31}P HRMAS NMR spectrum of **14i** (slurry in acetone, top), and ^{31}P NMR of **15** (solution in $CDCl_3$, bottom).

cis to Cl increases (Fig. 6, middle). Most likely, in the latter case each PPh_2 group is coordinated to a separate Rh center leading predominantly to the complex ($-PPh_2RhClCOD$). In this case, there are three Rh centers per tripodal linker. When using only one equivalent of RhClpyCOD the majority of the surface species assume a Wilkinson-type coordination of one Rh center, $(-PPh_2)_3RhCl$, resulting in a 1:2 ratio of the resonances at 40 ppm and 24 ppm (Fig. 6, top). It can be assumed that the coordination takes place randomly, and therefore, besides these clear-cut scenarios, a minor species with two coordinated PPh_2 groups, and coordination of phosphine groups from different, neighboring linkers to one Rh center cannot be ruled out.

To confirm the assumption that the pyridine ligand is most easily exchanged by a PPh_2 group, while the removal of COD is the second step, the coordination chemistry of **11** in solution was studied. Linker **6** reacts with one equivalent of RhClpyCOD in CH_2Cl_2 under dilute conditions (1 mM) to form a Wilkinson-type complex with ^{31}P resonances at 25.34 ppm (dd, $^1J(^{103}Rh\text{-}^{31}P) = 138.7$ Hz, $^2J(^{31}P\text{-}^{31}P) = 39.8$ Hz) and 37.54 ppm (dt, $^1J(^{103}Rh\text{-}^{31}P) = 193.6$ Hz, $^2J(^{31}P\text{-}^{31}P) = 39.8$ Hz). Upon concentration of the solution, an orange precipitate forms, which is insoluble in organic solvents. This can be explained by the formation of a coordination polymer with the Rh center featuring a node. Potential condensation of the siloxane groups [45], as observed during the purification of the linkers **4**-**6**, may contribute to the poor solubility. Employing three equivalents of RhClpyCOD with respect to **6** in CH_2Cl_2 yields complex **15** cleanly. **15** displays only a single ^{31}P NMR resonance at 26.14 ppm with a large $^1J(^{103}Rh\text{-}^{31}P)$ coupling of 147.9 Hz (Fig. 7, bottom). The preference to substitute the ligand *cis* to Cl prior to COD has been observed previously for the similar ligand $[CH_3P((CH_2)_7PPh_2)_3]^+ I^-$ [23], and this assumption is also in accord with a report by Gray et al. [46] In support of this interpretation, the ^{31}P HRMAS NMR spectrum of **14i** shows a clearly resolved doublet at 25.7 ppm with a $^1J(^{103}Rh\text{-}^{31}P)$ coupling constant of 148.7 Hz (Fig. 7, top).

Catalytic olefin hydrogenation

Few reactions in transition-metal catalysis have enjoyed a more detailed investigation than hydrogenation both in solution and on surfaces [35]. The hydrogenation of olefins in particular is of great importance for industrial applications and fundamental research. Therefore, the hydrogenation of 1-dodecene was chosen as a model system to investigate the catalytic activity of the functionalized silica **7i**-**9i** and **12i**-**14i** (Scheme 3). Another reason for this choice is that there is ample data obtained from the same experimental setting for this reaction, performed with different catalysts, that the new results can be compared with [23–26,35,36].

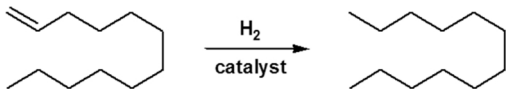

Scheme 3. Catalytic hydrogenation of 1-dodecene; pressure 1.1 atm, substrate : catalyst ratio 100 : 1, reaction temperature 60 °C.

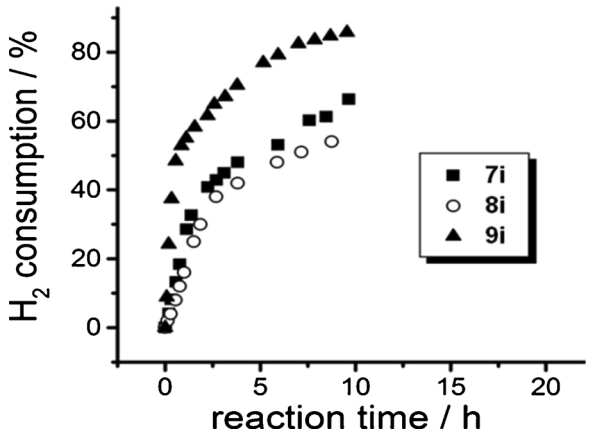

Fig. 8. Hydrogenation of 1-dodecene with the immobilized catalysts **7i**, **8i**, and **9i** in the first run.

Figs. 8 and 9 show the hydrogen uptake of **7i**-**9i** and **12i**-**14i**, respectively. The materials **7i**-**9i**, obtained by using Wilkinson's catalyst as precursor, show no induction period and lead to fast initial hydrogen uptake before slowing down after about three hours. The Rh complex **9i** with the longest methylene chain is the most active catalyst, confirming the assumption that the higher degree of mobility of the catalyst is the dominating factor that leads to the higher activity. Although one might speculate that the long linker chains can get entangled with each other or curl up and in this way increase the bulk of the linker, earlier results indicate that this is not the case [8,39g]. Long methylene chains (up to C_{18}), for example those incorporated in phosphine oxides are rather

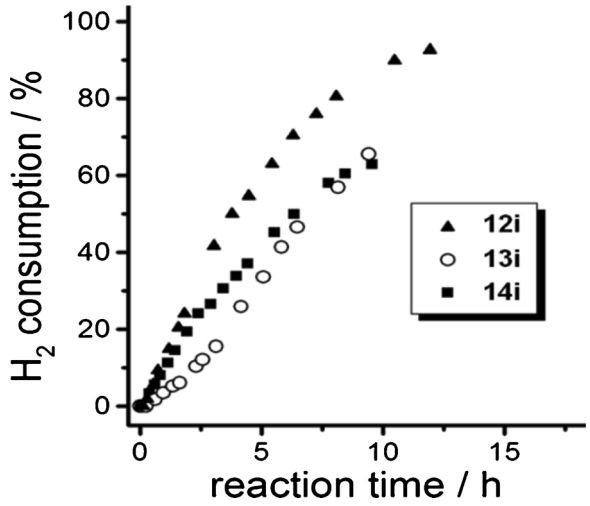

Fig. 9. Hydrogenation of 1-dodecene with the immobilized catalysts **12i**, **13i**, and **14i** in the first run.

rigid and extended linearly in one direction in single crystals [39g]. The phosphine oxides can be adsorbed on silica and solid-state NMR analysis shows that their methylene chains are spread out on the surface and do not get entangled [39g]. Therefore, even when bound covalently to a surface, and in the presence of a solvent, long methylene chains most probably do not curl up and become bulky, but extend linearly from the tetrahedral Si center. The surface coverages with the individual linker molecules were chosen low enough to prevent interactions with neighboring linker chains (Table 1). Furthermore, the small linewidths in the HRMAS spectra of the covalently bound linkers (Table 2) corroborate the assumption that the longest linker displays the highest mobility, speaking against getting entangled and bulky.

It is noteworthy to mention that all materials darken gradually and turn brown overnight. The complexes immobilized by linkers with chain lengths of four and seven methylene units, **7i** and **8i**, show comparable catalytic activities. Although they are less active than **9i** within the overall time frame, they reach 100% conversion of 1-dodecene to dodecane at about the same time, 27 h, *versus* 25 h for **9i**.

The activities of **12i**-**14i** in the first run are depicted in Fig. 9. Although their initial activities differ, all catalysts reach 100% substrate conversion at about 25 h reaction time. There is a significant difference as compared to the results of **7i**-**9i**, as all three materials show an induction period with no initial hydrogen uptake (Fig. 10). An induction period is characteristic for systems in which the employed metal complex is not an active catalyst itself and first needs to be transformed into another, active species. The new species can be a molecular complex, an aggregate, or a nanoparticle. Especially **13i** shows a sigmoidal hydrogen uptake curve, which has been described by Finke et al. as an indicator of nanoparticle formation [47]. Similar to the catalysts **7i**-**9i**, **12i**-**14i** also change color from yellow or slightly orange to black within the first run.

Two scenarios can explain these observations: **(a)** The induction period is due to the transformation of the molecular species into metal nanoparticles, which constitute the catalytically active species. **(b)** Alternatively, the immobilized Rh complexes still bearing COD as a ligand are not catalytically active and first have to undergo ligand dissociation to turn into active species. It is also possible that both scenarios **(a)** and **(b)** occur simultaneously.

Scenario **(b)** is supported by the observation that the length of the induction period is in the order of minutes and does not correlate with the color change of the materials that takes place within hours and is most evident after full conversion of the substrate. To investigate the role of the COD ligand, the hydrogen uptake of 1-dodecene with ClRh$(PPh_3)_3$ as the catalyst in the presence of two equivalents of COD was monitored. The solution was yellow, in contrast to the orange solution

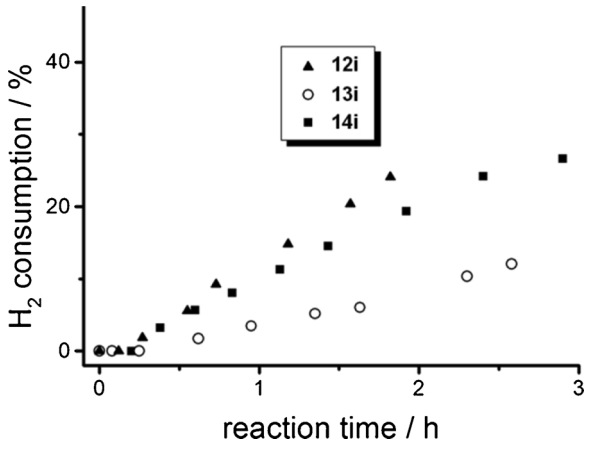

Fig. 10. Induction periods of the immobilized catalysts **12i**, **13i**, and **14i** during the initial three hours of the hydrogenation of 1-dodecene in the first run.

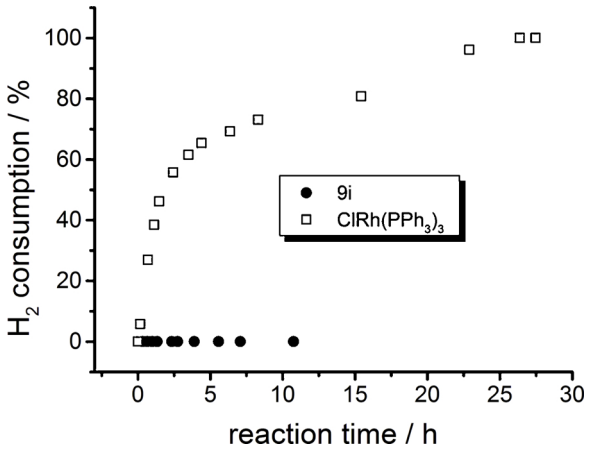

Fig. 11. Three-phase test using a batch of silica-immobilized allyltriethoxysilane in combination with **9i** and dissolved Wilkinson's catalyst.

in the absence of COD, and no hydrogen uptake was observed within the first ten hours. This might be due to reluctant dissociation of the COD ligand or due to the slow hydrogenation of the internal double bonds of COD [48]. These observations render scenario **(b)** highly likely as the reason for the induction period.

Next, the nature of the active species in the case of **7i**-**9i** was further investigated. A three-phase test similar to the one reported by Collman [49] and adapted to tethered catalyst systems by us previously [23] was carried out. Hereby, the olefinic substrate is not added to the reaction mixture but immobilized on a different batch of silica. Allyltriethoxysilane as the substrate is tethered to silica, and mixed with a different batch of silica, containing immobilized catalyst **9i**. Then, the solvent is added and hydrogen is offered. In case any Rh catalyst can leach into solution, it reaches the substrate, performs the catalysis and consumes hydrogen in the process. No hydrogen uptake is detected using **9i** as catalyst, proving that the catalytic activity is associated with the solid support and no active species leach into the solution (Fig. 11). When added to a slurry of the immobilized allyltriethoxysilane in a control experiment, Wilkinson's catalyst leads to 100% hydrogen consumption within 28 h (Fig. 11).

Next, we sought to better define the nature of the catalyst **9i** on the silica surface and determine whether it remains a homogeneous immobilized catalyst, or is tranformed into metal clusters or nanoparticles during catalysis. The formation of metal aggregates or nanoparticles is a common complicating factor in the area of immobilized molecular transition metal catalysts. This topic has been reviewed in detail by Finke et al. [47] and has also been observed in our group recently [19,23]. The Crabtree group has developed an elegant test to distinguish molecular hydrogenation catalysts from colloidal metal particles [50]. Carrying out hydrogenation reactions in the presence of DBCOT (dibenzo[*a,e*]cyclooctatetraene) efficiently poisons homogeneous metal catalysts. The chelating ligand DBCOT coordinates firmly to the metal center, and in this way it blocks open coordination sites for incoming substrate molecules. Therefore, homogeneous metal complexes, either in solution, or tethered to a support, will be poisoned, while the extended surfaces of metals or nanoparticles are not influenced by DBCOT. We successfully adapted this test earlier to distinguish between immobilized single site catalysts of a molecular nature and metal nanoparticles on a silica surface [23]. Analogously, we tested the hydrogenation of 1-dodecene using **9i** in the presence of two equivalents of DBCOT (Fig. 12). It is confirmed unequivocally that in the first run the immobilized catalyst **9i** is still of a homogeneous nature because it is poisoned by DBCOT and no longer catalytically active (Fig. 12). No hydrogen uptake or color change is observed over the course of ten hours. This result is important because it strengthens the assumption that initially the material consists of a molecular single site catalyst

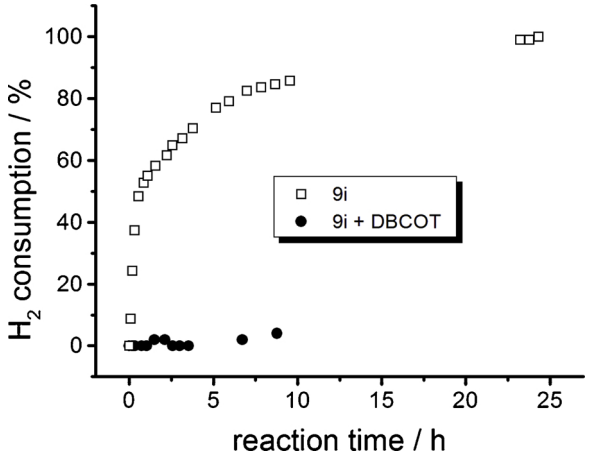

Fig. 12. Hydrogen consumption during the hydrogenation of 1-dodecene with **9i** in the presence of the poisoning agent DBCOT (dibenzo[*a,e*]cyclooctatetraene) and without it.

with three phosphine groups coordinating to the Rh center in a chelating manner.

Recycling of the catalysts

One of our main goals was to investigate whether the choice of precatalyst influences the recycling characteristic of the immobilized Rh catalysts. Therefore, **8i** and **13i** were targeted for the next series of experiments. For **8i** the ligand exchange was performed with Wilkinson's catalyst (Scheme 1), **13i** was derived from ClRhpyCOD (Scheme 2). Indeed, **8i** and **13i** showed distinctly different recycling characteristics that were studied by carrying out the hydrogenation of 1-dodecene in a batchwise manner. After complete conversion in each run, which typically took about 24 h, the functionalized material was allowed to settle and the supernatant was removed with a pipette. The supernatant was analyzed by GC and ^{1}H NMR to confirm full conversion. The functionalized silica was washed with toluene and employed for the subsequent catalytic run. In the case of **8i** the catalytic activity is high throughout the first 4 h, compared to Wilkinson's catalyst under the same conditions, before a distinct drop in the activity takes place (Fig. 13). In the subsequent runs the activity increases and reaches a maximum in the 5th run, after which the activity begins to decrease slightly with each catalytic run. In cycle 5 the rates are most probably higher because the homogeneous catalyst still persists and is performing the catalytic reaction, together with the added activity of the

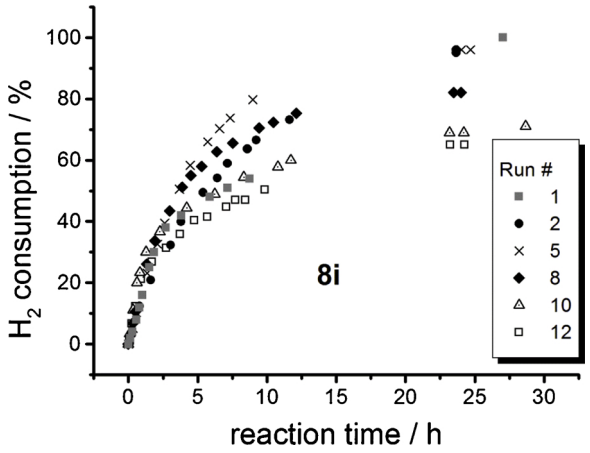

Fig. 13. Hydrogen consumption during 12 batchwise catalytic runs with **8i**. Only selected runs are shown for clarity.

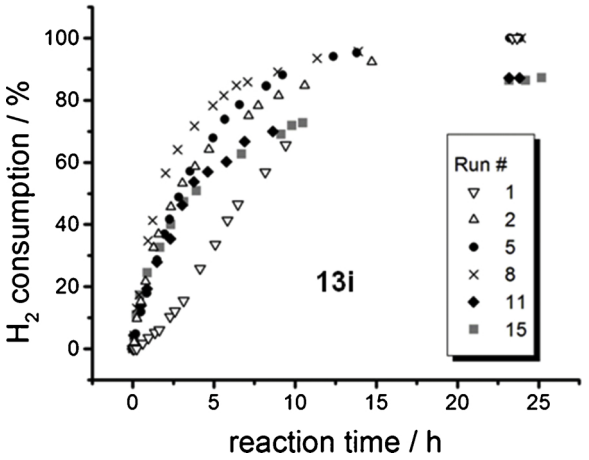

Fig. 14. Hydrogen consumption during 15 batchwise catalytic runs using **13i**. Only selected runs are shown for clarity.

most active, small Rh nanoparticles. In the following runs, the activity decreases again because the homogeneous form of the immobilized catalyst does no longer exist and only the larger, catalytically less active nanoparticles perform the catalytic reaction. A similar outcome has been observed earlier with other linker systems [23,24,31].

For **13i** the difference between the first and the following runs is even more drastic (Fig. 14). The hydrogen uptake in the first run is sigmoidal and shows a distinct induction period which is not observed in the second and the following runs. In analogy to **8i**, the activity increases in the first catalytic cycles, reaching its maximum around the 8th run and then decreases to reach a plateau after the 11th run.

In order to check an earlier observation made when studying an immobilized Rh catalyst with **10i** as the linker [23], we exposed catalyst **7i** to air while stirring the slurry in toluene for 24 h between the 6th and 7th catalytic run. No decrease of the catalytic activity was found, in analogy to the previously reported case [23]. This is favorable with respect to catalyst handling and a potential industrial application. It also suggests, however, that the active species at that stage is not a molecular single site catalyst anymore, since phosphine complexes of Rh are highly air-sensitive in solution and prone to ligand oxidation.

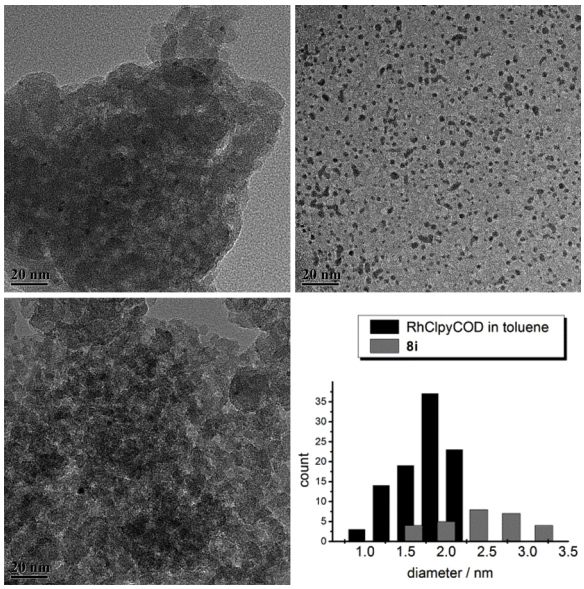

Fig. 15. TEM images of the Rh nanoparticles formed during catalysis with **7i** (bottom left, after exposure to air), **8i** (top left), and ClRhpyCOD (top right) in toluene and their corresponding size distributions (bottom right).

The catalysts **7i** and **8i** were therefore subjected to TEM analyses (Fig. 15). **7i** was analyzed after 7 catalytic runs, being exposed to air after the sixth run, and **8i** after 12 runs. In both cases Rh nanoparticles were detected on the outside surface of the particles, or within the pores of the silica support [14,23,51]. The average size of the nanoparticles is about 2.5 nm in the case of **8i**, with a broad size distribution from 1.5 to 3.5 nm. For **7i** nanoparticles are observed as well, but not enough nanoparticles could be identified to estimate an average size or size distribution. The reaction mixture using ClRhpyCOD (**11**) as a homogeneous metal precatalyst for comparison was also analyzed. Interestingly, using ClRhpyCOD for catalytic hydrogenation led to the formation of highly dispersed Rh nanoparticles with a narrow size distribution centered at 1.7 nm. The nanoparticles stay suspended in toluene for at least two weeks without noticeable aggregation. A similar observation has recently been made with a homogeneous Ni catalyst coordinated by a tripodal triphosphine ligand that had been used for the cyclotrimerization of phenylacetylene [19].

For all immobilized catalysts, the results of the TEM analyses in combination with the spectroscopic data and poisoning experiments suggest that the initial catalytically active species is a well-defined molecular single site metal complex that is highly active for the hydrogenation of 1-dodecene. In the course of several hours these species gradually decompose to form surface-supported Rh nanoparticles which also constitute active hydrogenation catalysts [14,23]. In contrast to electrostatically bound linkers, the phosphines incorporating ethoxysilane groups are covalently bound to their specific surface site. Therefore, the results show that the metal atoms do not have to be delivered to the nanoparticles directly by the phosphine linkers. After being detached from the linkers, the metal atoms can be stabilized by the solvent and migrate through the solution, or along the solution/surface interface to finally assemble as nanoparticles on the surface. This process would explain the absence of nanoparticles in solution, when immobilized catalysts are studied. A substantial amount of metal has never been detected in the supernatant of immobilized catalysts by AAS. Additionally, the recent ^{31}P HRMAS NMR studies of a $PdCl_2$ fragment migrating over the lawn of immobilized chelating phosphines on silica that was only wetted with a solvent in the course of several hours corroborates this assumption [20–22].

Conclusion

Six new tripodal phosphine linkers incorporating long methylene chains $(CH_2)_{4\text{-}11}$ and their precursor ethoxysilanes have been synthesized and fully characterized. The linkers have been successfully immobilized on silica and characterized by ^{31}P and ^{29}Si CP/MAS NMR. ^{31}P HRMAS measurements in the presence of solvents revealed that the mobilities of the linker chains increase with their lengths. However, a comparison with an analogous linker bound to silica by electrostatic interactions indicates that the ethoxysilane-containing linkers do not have translational mobility, but remain firmly rooted at their specific surface sites. Surface-bound Wilkinson-type Rh complexes have been obtained with the immobilized linkers by ligand exchange with $ClRh(PPh_3)_3$ and ClRhpyCOD. In the latter case the pyridine ligand is exchanged more easily than COD, as proven by investigating the molecular coordination chemistry in solution. Further proof of the coordination comes from the well-resolved ^{31}P HRMAS spectrum of an immobilized Rh complex which shows a clearly resolved $^1J(^{103}Rh\text{-}^{31}P)$ coupling. The single crystal X-ray structure of ClRhpyCOD has been described. The olefin hydrogenation catalysis results demonstrate that the initial catalytically active species is molecular in nature, with a well-defined coordination environment. Under hydrogenation conditions these single site species are transformed into nanoparticles on the time scale of several hours. Since the phosphine linkers that are covalently bound to the support by ethoxysilane groups do not move from their specific surface sites, it is suggested that translational mobility of the entire linker/metal complex assembly is not a prerequisite for metal aggregation or nanoparticle formation. Most likely, also in the context of earlier results on the time frame of metal complex migration [20–22], the metal centers are stabilized by the solvent after leaving the linkers and migrate in the solvent/support interface to an aggregate or nanoparticle, where they finally deposit. The time frame and outcome of the migration depends on the specific coordination of the Rh centers. The timeline of nanoparticle formation has been defined by three-phase and catalyst poisoning tests. The size distributions of the nanoparticles has been obtained by TEM images. Importantly, all immobilized Rh catalysts can be recycled at least 15 times in a batchwise manner while remaining active, even in air.

In summary, immobilized catalysts still represent a young, but growing field. Its importance can hardly be overestimated and many immobilized catalyst systems have already been proven successful, in our group and others. The presented new linker system adds key outcomes to earlier studies. Although the ideal catalyst [1] might not yet have been found, just comparing, for example, any of the immobilized catalysts in this work with homogeneous Wilkinson's catalyst shows the advantage. Wilkinson's catalyst cannot be removed from the reaction mixture without tedious purification procedures and corresponding loss of product. It also cannot be recycled, and it is air sensitive. The immobilized catalysts **7i-9i** and **12i-14i**, on the other hand, can be recycled at least 15 times, they are not air sensitive once they are completely transformed into nanoparticles, and they can be removed from the reaction mixture at any stage without product loss by simple decanting of the solvent and product after the catalyst has settled within 5 min. Immobilized catalysts also have the potential to be applied in continuous settings, which is impossible with homogeneous catalysts.

A more systematic study of the nanoparticle growth and size distribution, using tripodal phosphine linkers with shorter methylene chains [19], will shed light on the correlation with the changes in catalytic activity in future studies.

Experimental section

General remarks

The ^{1}H, ^{13}C, and ^{31}P NMR spectra of liquids were recorded at 499.7, 125.7, and 202.3 MHz on a 500 MHz Varian spectrometer and referenced as follows: ^{1}H: residual internal $CHCl_3$ (δ, 7.26 ppm), $CDHCl_2$ (δ, 5.32 ppm), or C_6D_5H (δ, 7.16 ppm); ^{13}C: internal $CDCl_3$ (δ, 77.23 ppm) or C_6D_6 (δ, 128.06 ppm). ^{31}P NMR spectra were referenced with respect to neat Ph_2PCl (δ, 81.92 ppm) in a capillary, which was centered in the NMR sample tube. The ^{13}C and ^{31}P NMR spectra were recorded with ^{1}H decoupling. ^{29}Si NMR spectra of liquids were measured at 79.37 MHz on a 400 MHz Varian spectrometer and referenced with respect to external hexamethyldisiloxane ($Me_3SiOSiMe_3$) in $CDCl_3$ (δ, 6.53 ppm). The solid-state NMR spectra were measured with a Bruker Avance 400 widebore NMR spectrometer equipped with 4 and 7 mm MAS probeheads. The dry samples were filled loosely into the ZrO_2 rotors as powders. The HRMAS samples were prepared by filling the dry samples into commercially available Bruker HRMAS rotors featuring spacers at the top and bottom, and a slight excess of solvent was added. After the silica settled, the excess supernatant was removed, leaving enough solvent to cover the solid. During the ^{31}P HRMAS, CP/MAS, and MAS data acquisition ^{1}H high-power decoupling was applied. The recycle delays were 5 s for HRMAS and CP/MAS, and 10 s for MAS spectra. The ^{13}C and ^{29}Si solid-state NMR spectra were referenced with respect to external adamantane and $(Me_3Si)_4Si$, respectively, which were also used for optimizing the Hartmann-Hahn matching conditions. ^{31}P solid-state NMR spectra were referenced with respect to external $NH_4H_2PO_4$ (δ, +0.81 ppm). GC analyses were carried out on a Shimadzu GC 2010 gas chromatograph equipped with a SHRXI-5MS column (15 m × 0.25 mm × 0.25 μm) and a flame ionization detector (GC-FID). TEM images were obtained on an FEI Tecnai G2 F20 microscope and ImageJ software was used to determine the particle size distribution. Melting

points were recorded with a Stanford Research Systems (SRS) MPA100 (Opti-Melt) automated melting point system.

Single crystals of ClRhpyCOD (**11**) were grown from MeCN. A suitable crystal was selected and measured on a Bruker APEX-II CCD diffractometer. The crystal was kept at 150 K during data collection. Using Olex2 [52], the structure was solved with the ShelXT [53] structure solution program using Intrinsic Phasing and refined with the ShelXL [54] refinement package using Least Squares minimization.

All reactions were carried out using standard Schlenk techniques and a purified N_2 atmosphere, if not stated otherwise. Reagents purchased from Sigma Aldrich or VWR were used without further purification. Solvents were dried by boiling them over Na, distilled, and stored under N_2. CH_2Cl_2 was obtained from a solvent purification system. The silica used for immobilizations (Merck, 40 Å average pore diameter, particle size 0.063 to 0.2 mm, specific surface area 750 m^2/g) was rigorously dried *in vacuo* at 300 °C for 4 days to remove adsorbed water and condense surface silanol groups. For chromatographic purification of compounds the silica was used as received. The purity of the molecular ethoxysilanes was confirmed by their ^1H, ^{13}C, ^{29}Si, and ^{31}P NMR spectra (see Supplementary Material), since they possess no characteristic IR bands and are viscous oils that do not crystallize.

General procedure A – immobilization

Method A

Phosphine **4** (294 mg, 0.368 mmol) is dissolved in toluene (10 ml) and added to a slurry of SiO_2 (1.169 g) with toluene (40 ml). The mixture is stirred overnight at 70 °C before the silica is allowed to settle and the supernatant is decanted. The functionalized silica is washed twice with toluene (20 ml) and twice with CH_2Cl_2 (20 ml). Then the silica is dried *in vacuo* at RT for 3 h. The supernatant and the washing phases are combined and the solvent is removed *in vacuo*. The residue is weighed and analyzed by ^{31}P and ^1H NMR. The surface coverage is determined gravimetrically by measuring the weight increase of the silica and the weight of the excess ligand in the supernatant and washing phases.

Method B

Phosphine **4** (436 mg, 0.547 mmol) is dissolved in toluene (15 ml). Then 3 ml of a 1 M solution of $H_3B{\cdot}THF$ in THF is added and the solution is stirred for 30 min. The solvent is removed *in vacuo*, the residue redissolved in toluene (10 ml), and added to a slurry of SiO_2 (3.449 g) with toluene (40 ml). The mixture is stirred for 48 h at 60 °C, before the silica is allowed to settle and the supernatant is decanted. Subsequently, the functionalized silica is washed twice each with toluene (20 ml) and CH_2Cl_2 (20 ml), and dried *in vacuo* for 3 h. The supernatant and the washing phases are combined and the solvent is removed *in vacuo*. The residue is checked by ^{31}P and ^1H NMR. The surface coverage is determined gravimetrically by measuring the weight increase of the silica and the excess ligand in the combined liquid phases. Then, a solution of DABCO (187 mg, 1.667 mmol) in toluene (10 ml) is added to the slurry of the functionalized silica and the mixture is stirred at RT for 24 h. Finally, the supernatant is decanted and the silica is washed twice with CH_2Cl_2 (20 ml), before being dried *in vacuo* at room temperature for 3 h.

General procedure B – hydrogenation

Immobilized catalyst **9i** (347 mg, 0.010 mmol Rh) is mixed with 4 ml of toluene in a Schlenk flask, which is then attached to the hydrogenation apparatus [25] and heated to 60 °C. To start the catalytic reaction 1-dodecene (168.3 mg, 1 mmol), dissolved in toluene (1 ml), is added to the slurry with a syringe through the stopcock. Then the mixture is stirred at 750 rpm and the hydrogen uptake is monitored. After complete substrate conversion the silica is allowed to settle. The supernatant is removed *via* syringe and the silica is washed twice with 4 ml of toluene. The supernatant is analyzed by GC and ^1H NMR to confirm 100% substrate conversion.

Synthesis and characterization

*Tris(but-3-enyl)ethoxysilane **1***

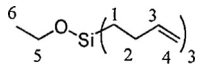

Mg shavings (670 mg, 26.56 mmol) are suspended in Et_2O (20 ml) and bromobut-3-ene (2.622 g, 19.4 mmol) is added dropwise. The reaction mixture is stirred at RT for 3 h. Then the Grignard reagent is added to $EtOSiCl_3$ (861 mg, 4.692 mmol), dissolved in Et_2O (20 ml), at 0 °C *via* a cannula. The reaction mixture is allowed to warm to RT and then stirred for 2 h. Subsequently, 20 ml of the solvent are removed *in vacuo* and 20 ml of hexanes are added to precipitate the salts formed during the Grignard reaction. The reaction mixture is filtered through celite and the solvent is removed *in vacuo*. The crude product is purified by column chromatography (SiO_2, hexanes : ethylacetate = 8 : 1) and **1** (514 mg, 2.158 mmol) is obtained from the first fraction as a colorless liquid in 46% yield. The colorless liquid hexa(but-3-enyl)disiloxane **1b** (94 mg, 0.233 mmol) is isolated as a minor product from the second fraction in 10% yield.

*Tris(but-3-enyl)ethoxysilane **1***

^1H NMR ($CDCl_3$, 499.7 MHz): δ (ppm) = 5.88 (ddt, $^3J_{trans}(^1H\text{-}^1H)$ = 16.4 Hz, $^3J_{cis}(^1H\text{-}^1H)$ = 10.1 Hz, $^3J(^1H\text{-}^1H)$ = 6.3 Hz, 3H, H3), 4.99 (ddt, $^3J_{trans}(^1H\text{-}^1H)$ = 17.0 Hz, $^2J(^1H\text{-}^1H)$ = 3.5 Hz, $^4J(^1H\text{-}^1H)$ = 1.7 Hz, 3H, $H4_Z$), 4.87 (tdd, $^3J_{cis}(^1H\text{-}^1H)$ = 10.1 Hz, $^2J(^1H\text{-}^1H)$ = 3.2 Hz, $^4J(^1H\text{-}^1H)$ = 1.4 Hz, 3H, $H4_E$), 3.68 (q, $^3J(^1H\text{-}^1H)$ = 6.9 Hz, 2H, H5), 2.07–2.13 (m, 6H, H2), 1.18 (t, $^3J(^1H\text{-}^1H)$ = 6.9 Hz, 3H, H6), 0.71-0.76 (m, 6H, H1); **$^{13}C\{^1H\}$ NMR** ($CDCl_3$, 125.7 MHz): δ (ppm) = 141.50 (C3), 111.10 (C4), 58.53 (C5), 27.64 (C2), 18.08 (C6), 13.18 (C1); **$^{29}Si\{^1H\}$ NMR** ($CDCl_3$, 79.4 MHz): δ (ppm) = 14.70 (s).

*Hexakis(but-3-enyl)disiloxane **1d***

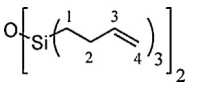

^1H NMR ($CDCl_3$, 499.7 MHz): δ (ppm) = 5.89 (ddt, $^3J_{trans}(^1H\text{-}^1H)$ = 16.5 Hz, $^3J_{cis}(^1H\text{-}^1H)$ = 10.1 Hz, $^3J(^1H\text{-}^1H)$ = 6.3 Hz, 6H, H3), 5.01 (ddt, $^3J_{trans}(^1H\text{-}^1H)$ = 17.1 Hz, $^2J(^1H\text{-}^1H)$ = 3.5 Hz, $^4J(^1H\text{-}^1H)$ = 1.7 Hz, 6H, $H4_Z$), 4.91 (ddt, $^3J_{cis}(^1H\text{-}^1H)$ = 10.1 Hz, $^2J(^1H\text{-}^1H)$ = 3.2 Hz, $^4J(^1H\text{-}^1H)$ = 1.3 Hz, 6H, $H4_E$), 2.10–2.16 (m, 12H, H2), 0.70-0.76 (m, 12H, H1); **$^{13}C\{^1H\}$ NMR** ($CDCl_3$, 125.7 MHz): δ (ppm) = 141.13 (C3), 113.08 (C4), 27.01 (C2), 14.01 (C1).

*Tris(hept-6-enyl)ethoxysilane **2***

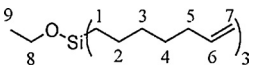

Mg shavings (939 mg, 38.6 mmol) are suspended in Et_2O (20 ml) and 1-bromohept-6-ene (3.385 g, 19.115 mmol) is added dropwise. The reaction mixture is stirred at RT for 3 h. Then the Grignard reagent is added to $EtOSiCl_3$ (945 mg, 5.150 mmol), dissolved in Et_2O (20 ml), at 0 °C *via* cannula. The reaction mixture is allowed to warm to RT and then stirred for 2 h. Subsequently, 20 ml of the solvent are removed *in vacuo* and 20 ml of hexanes are added to precipitate the salts formed during the Grignard reaction. The reaction mixture is filtered through celite and the solvent removed *in vacuo*. The crude product is purified by column chromatography (SiO_2, hexanes : ethylacetate = 8 : 1) and **2**

(523 mg, 1.434 mmol) is obtained as a colorless liquid in 28% yield from the first fraction. The colorless liquid **2d** (510 mg, 0.778 mmol) is isolated from the second fraction as the major product in 30% yield.

*Tris(hept-6-enyl)ethoxysilane **2***

^{1}H NMR ($CDCl_3$, 499.7 MHz): δ (ppm) = 5.81 (ddt, $^3J_{trans}$(^{1}H-^{1}H) = 16.9, 3 Hz, $^3J_{cis}$(^{1}H-^{1}H) = 10.2 Hz, ^3J(^{1}H-^{1}H) = 6.7 Hz, 3H, H6), 4.99 (ddt, $^3J_{trans}$(^{1}H-^{1}H) = 17.1 Hz, ^2J(^{1}H-^{1}H) = 2.1 Hz, ^4J(^{1}H-^{1}H) = 1.5 Hz, 3H, H7$_Z$), 4.93 (ddt, $^3J_{cis}$(^{1}H-^{1}H) = 10.2 Hz, ^2J(^{1}H-^{1}H) = 2.3 Hz, ^4J(^{1}H-^{1}H) = 1.1 Hz, 3H, H7$_E$), 3.65 (q, ^3J(^{1}H-^{1}H) = 6.9 Hz, 2H, H8), 2.00–2.07 (m, 6H, H5), 1.30–1.41 (m, 18H, overlapping H2, H3, H4), 1.17 (t, ^3J(^{1}H-^{1}H) = 6.9 Hz, 2H, H9), 0.56-0.61 (m, 6H, H1); **^{13}C{^{1}H} NMR** ($CDCl_3$, 125.7 MHz): δ (ppm) = 139.21 (C6), 114.11 (C7), 58.37 (C8), 33.73 (C5*), 33.11 (C3*), 28.57 (C4), 23.02 (C2), 18.65 (C9), 13.59 (C1), *assignments interchangeable; **^{29}Si{^{1}H} NMR** ($CDCl_3$, 79.4 MHz): δ (ppm) = 15.36 (s).

*Hexakis(hept-6-enyl)disiloxane **2d***

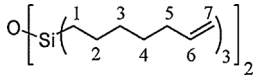

^{1}H NMR ($CDCl_3$, 499.7 MHz): δ (ppm) = 5.81 (ddt, $^3J_{trans}$(^{1}H-^{1}H) = 16.9 Hz, $^3J_{cis}$(^{1}H-^{1}H) = 10.2 Hz, ^3J(^{1}H-^{1}H) = 6.7 Hz, 6H, H6), 4.99 (ddt, $^3J_{trans}$(^{1}H-^{1}H) = 17.1 Hz, ^2J(^{1}H-^{1}H) = 2.1 Hz, ^4J(^{1}H-^{1}H) = 1.5 Hz, 6H, H7$_Z$), 4.93 (ddt, $^3J_{cis}$(^{1}H-^{1}H) = 10.2 Hz, ^2J(^{1}H-^{1}H) = 2.2 Hz, ^4J(^{1}H-^{1}H) = 1.2 Hz, 6H, H7$_E$), 2.04 (dt, ^3J(^{1}H-^{1}H) = 6.7 Hz, ^3J(^{1}H-^{1}H) = 6.6 Hz, 12H, H5), 1.30–1.43 (m, 36H, overlapping H2, H3, H4), 0.56-0.61 (m, 12H, H1); **^{13}C{^{1}H} NMR** ($CDCl_3$, 125.7 MHz): δ (ppm) = 139.16 (C6), 114.15 (C7), 33.69 (C5*), 33.01 (C3*), 28.57 (C4), 22.91 (C2), 14.99 (C1), *assignments interchangeable.

*Tris(undec-10-enyl)ethoxysilane **3***

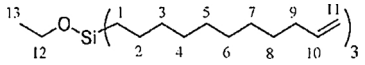

Mg shavings (980 mg, 40.31 mmol) are suspended in THF (20 ml) and bromoundec-10-ene (3.757 g, 16.11 mmol) is added dropwise. The reaction mixture is stirred at RT for 3 h. Then the Grignard reagent is added to $EtOSiCl_3$ (738 mg, 4.022 mmol) in THF (20 ml) at 0 °C *via* cannula. The reaction mixture is allowed to warm to RT and stirred for 2 more h. Then 20 ml of the solvent is removed *in vacuo* and 20 ml of hexanes are added to precipitate the salts formed during the Grignard reaction. The reaction mixture is filtered through celite and the solvent is removed *in vacuo*. The crude product is purified by column chromatography (SiO_2, hexanes : ethylacetate = 19 : 1) to give **3** (1.163 g, 2.181 mmol) as a colorless liquid in 54% yield. The minor product hexakis(undec-10-enyl)disiloxane **3b** (43 mg, 0.043 mmol) is isolated as a colorless liquid in 2% yield.

*Tris(undec-10-enyl)ethoxysilane **3***

^{1}H NMR ($CDCl_3$, 499.7 MHz): δ (ppm) = 5.81 (ddt, $^3J_{trans}$(^{1}H-^{1}H) = 16.9 Hz, $^3J_{cis}$(^{1}H-^{1}H) = 10.2 Hz, ^3J(^{1}H-^{1}H) = 6.7 Hz, 3H, H10), 4.99 (ddt, $^3J_{trans}$(^{1}H-^{1}H) = 17.1 Hz, ^2J(^{1}H-^{1}H) = 3.7 Hz, ^4J(^{1}H-^{1}H) = 1.6 Hz, 3H, H11$_Z$), 4.92 (ddt, $^3J_{cis}$(^{1}H-^{1}H) = 10.2 Hz, ^2J(^{1}H-^{1}H) = 2.3 Hz, ^4J(^{1}H-^{1}H) = 1.2 Hz, 3H, H11$_E$), 3.66 (q, ^3J(^{1}H-^{1}H) = 6.9 Hz, 2H, H12), 2.04 (dtt, ^3J(^{1}H-^{1}H) = 7.7 Hz, ^3J(^{1}H-^{1}H) = 6.8 Hz, ^4J(^{1}H-^{1}H) = 1.3 Hz, 6H, H9), 1.37 (m, 6H, H8), 1.24–1.32 (m, 36H, H2-H7), 1.17 (t, ^3J(^{1}H-^{1}H) = 6.9 Hz, 3H, H13), 0.58-0.61 (m, 6H, H1); **^{13}C{^{1}H} NMR** ($CDCl_3$, 125.7 MHz): δ (ppm) = 139.18 (C10), 114.06 (C11), 58.33 (C12), 33.82 (C8*), 33.66 (C9*), 29.54 (two overlapping signals, C3°, C5°), 29.29 (C4°), 29.16 (C6°), 28.96 (C7°), 23.17 (C2), 18.65 (C13), 13.64 (C1), *,°interchangeable assignments; **^{29}Si{^{1}H} NMR** ($CDCl_3$, 79.4 MHz): δ (ppm) = 15.47 (s).

*Hexakis(undec-10-enyl)disiloxane **3d***

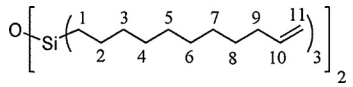

^{1}H NMR ($CDCl_3$, 499.7 MHz): δ (ppm) = 5.81 (ddt, $^3J_{trans}$(^{1}H-^{1}H) = 16.9 Hz, $^3J_{cis}$(^{1}H-^{1}H) = 10.2 Hz, ^3J(^{1}H-^{1}H) = 6.7 Hz, 6H, H10), 4.99 (ddt, $^3J_{trans}$(^{1}H-^{1}H) = 17.1 Hz, ^2J(^{1}H-^{1}H) = 3.6 Hz, ^4J(^{1}H-^{1}H) = 1.6 Hz, 6H, H11$_Z$), 4.91–4.95 (m, 6H, H11$_E$), 2.04 (dtt, ^3J (^{1}H-^{1}H) = 7.7 Hz, ^3J (^{1}H-^{1}H) = 6.9 Hz, ^4J(^{1}H-^{1}H) = 1.2 Hz, 12H, H9), 1.23–1.41 (m, 84H, H2-H8), 0.55-0.60 (m, 12H, H1).

*Tris(4-diphenylphosphinobutyl)ethoxysilane **4***

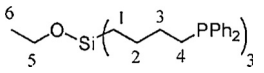

The ethoxysilane **1** (239 mg, 1.002 mmol), AIBN (44 mg, 0.267 mmol) and Ph_2PH (748 mg, 4.211 mmol) are combined in a Schlenk flask, heated to 70 °C and stirred for 4 d. The conversion is monitored by ^{31}P NMR of the reaction mixture. After completion of the reaction all volatile components are removed *in vacuo* and the crude product is purified by column chromatography (SiO_2, toluene) to give **4** (588 mg, 0.737 mmol) as a colorless viscous oil in 74% yield.

^{1}H NMR (C_6D_6, 499.7 MHz): δ (ppm) = 7.44–7.49 (m, 12H, H$_o$), 7.02–7.12 (m, 18H, H$_p$, H$_m$), 3.49 (q, ^3J(^{1}H-^{1}H) = 6.9 Hz, 2H, H5), 2.00–2.05 (m, 6H, H4), 1.51–1.60 (m, 6H, H3), 1.42–1.51 (m, 6H, H2), 1.11 (t, ^3J(^{1}H-^{1}H) = 6.9 Hz, 2H, H6), 0.49-0.54 (m, 6H, H1); **^{13}C{^{1}H} NMR** (C_6D_6, 125.7 MHz): δ (ppm) = 139.99 (d, ^1J(^{31}P-^{13}C) = 14.7 Hz, C$_i$), 133.15 (d, ^2J(^{31}P-^{13}C) = 18.5 Hz, C$_o$), 128.68 (d, ^3J(^{31}P-^{13}C) = 6.4 Hz, C$_m$), 128.61 (C$_p$), 58.49 (C5), 30.33 (d, ^2J(^{31}P-^{13}C) = 15.9 Hz, C3), 28.33 (d, ^1J(^{31}P-^{13}C) = 12.7 Hz, C4), 25.29 (d, ^3J(^{31}P-^{13}C) = 13.1 Hz, C2), 18.97 (C6), 13.87 (C1); **^{31}P{^{1}H} NMR** (C_6D_6, 202.3 MHz): δ (ppm) = -16.39 (s); **^{29}Si{^{1}H} NMR** ($CDCl_3$, 79.4 MHz): δ (ppm) = 12.21 (s).

*Hexakis(4-diphenylphosphinobutyl)disiloxane **4d***

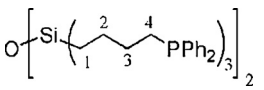

The disiloxane **1b** (389 mg, 0.965 mmol), AIBN (104 mg, 0.633 mmol) and Ph_2PH (1.157 g, 6.215 mmol) are combined in a Schlenk flask, heated to 70 °C and stirred for 5 d. After complete conversion, as monitored by ^{31}P NMR of the reaction mixture, the volatile components are removed *in vacuo* and the crude product is purified by column chromatography (SiO_2, pentane : ethylacetate = 4 : 1) to give **4d** (1.095 g, 0.720 mmol) as a colorless viscous oil in 75% yield.

^{1}H NMR (C_6D_6, 499.7 MHz): δ (ppm) = 7.45–7.49 (m, 24H, H$_o$), 7.03–7.12 (m, 36H, H$_p$, H$_m$), 1.99–2.04 (m, 12H, H4), 1.48–1.58 (m, 12H, H3), 1.37–1.45 (m, 12H, H2), 0.40-0.45 (m, 12H, H1); **^{13}C{^{1}H} NMR** (C_6D_6, 125.7 MHz): δ (ppm) = 139.98 (d, ^1J(^{31}P-^{13}C) = 14.6 Hz, C$_i$), 133.16 (d, ^2J(^{31}P-^{13}C) = 18. 6 Hz, C$_o$), 128.69 (d, ^3J(^{31}P-^{13}C) = 6.4 Hz, C$_m$), 128.63 (C$_p$), 30.23 (d, ^2J(^{31}P-^{13}C) = 15.8 Hz, C3), 28.32 (d, ^1J(^{31}P-^{13}C) = 12.8 Hz, C4), 25.09 (d, ^3J(^{31}P-^{13}C) = 13.0 Hz, C2), 15.16 (C1); **^{31}P{^{1}H} NMR** (C_6D_6, 202.3 MHz): δ (ppm) = −16.43 (s); **^{29}Si{^{1}H} NMR** ($CDCl_3$, 79.4 MHz): δ (ppm) = 15.73 (s).

*Tris(7-diphenylphosphinoheptyl)ethoxysilane **5***

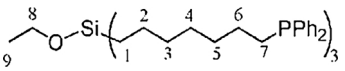

The ethoxysilane **2** (480 mg, 1.316 mmol), AIBN (94 mg, 0.572 mmol) and Ph_2PH (942 mg, 5.060 mmol) are combined in a Schlenk flask, heated to 70 °C and stirred for 5 d. The conversion is monitored by ^{31}P NMR of the reaction mixture. After completion of the reaction the crude product is purified by column chromatography (SiO_2, toluene) and **5** (538 mg, 0.582 mmol) is obtained as a colorless viscous oil in 44% yield.

^{1}H NMR (C_6D_6, 499.7 MHz): δ (ppm) = 7.45 (dd, $^3J(^{31}P\text{-}^1H)$ = 6.9 Hz, $^3J(^1H\text{-}^1H)$ = 6.9 Hz, 12H, H_o), 7.03–7.12 (m, 18H, H_m, H_p), 3.64 (q, $^3J(^1H\text{-}^1H)$ = 6.9 Hz, 2H, H8), 1.95–2.00 (m, 6H, H7), 1.42–1.51 (m, 12H, H6*, H5*), 1.31–1.39 (m, 12H, H4*, H3*), 1.24–1.31 (m, 6H, H2), 1.18 (t, $^3J(^1H\text{-}^1H)$ = 6.9 Hz, 3H, H9), 0.66-0.71 (m, 6H, H1), *assignments interchangeable; **^{13}C{^{1}H} NMR** (C_6D_6, 125.7 MHz): δ (ppm) = 140.02 (d, $^1J(^{31}P\text{-}^{13}C)$ = 14.7 Hz, C_i), 133.14 (d, $^2J(^{31}P\text{-}^{13}C)$ = 18.5 Hz, C_o), 128.67 (d, $^3J(^{31}P\text{-}^{13}C)$ = 6.4 Hz, C_m), 128.59 (C_p), 58.52 (C8), 34.06 (C3), 31.59 (d, $^3J(^{31}P\text{-}^{13}C)$ = 12.6 Hz, C5), 29.42 (C4), 28.63 (d, $^1J(^{31}P\text{-}^{13}C)$ = 12.4 Hz, C7), 25.51 (d, $^2J(^{31}P\text{-}^{13}C)$ = 16.3 Hz, C6), 23.76 (C2), 18.67 (C9), 14.26 (C1); **^{31}P{^{1}H} NMR** (C_6D_6, 202.3 MHz): δ (ppm) = -16.38 (s); **^{29}Si{^{1}H} NMR** (C_6D_6, 79.4 MHz): δ (ppm) = 13.93 (s).

*Hexakis(7-diphenylphosphinoheptyl)disiloxane **5d***

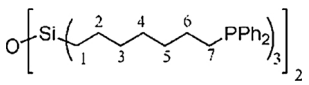

The disiloxane **2b** (465 mg, 0.709 mmol), AIBN (88 mg, 0.535 mmol) and Ph_2PH (1.187 g, 6.376 mmol) are combined in a Schlenk flask, heated to 70 °C and stirred for 5 d. The conversion is monitored by ^{31}P NMR of the reaction mixture. Upon completion of the reaction the crude product is purified by column chromatography (SiO_2, toluene : ethylacetate = 9 : 1) to give **5d** (855 mg, 0.502 mmol) as a colorless viscous oil in 70% yield.

^{1}H NMR (C_6D_6, 499.7 MHz): δ (ppm) = 7.44–7.49 (m, 24H, H_o), 7.03–7.14 (m, 36H, H_m, H_p), 1.96–2.01 (m, 12H, H7), 1.43–1.53 (m, 12H, H6*), 1.34–1.42 (m, 24H, H5*, H4*), 1.27–1.34 (m, 12H, H3*), 1.20–1.27 (m, 12H, H2), 0.56-0.61 (m, 12H, H1), *assignments interchangeable; **^{13}C{^{1}H} NMR** (C_6D_6, 125.7 MHz): δ (ppm) = 140.01 (d, $^1J(^{31}P\text{-}^{13}C)$ = 14.6 Hz, C_i), 133.14 (d, $^2J(^{31}P\text{-}^{13}C)$ = 18.5 Hz, C_o), 128.68 (d, $^3J(^{31}P\text{-}^{13}C)$ = 6.4 Hz, C_m), 128.60 (C_p), 33.95 (C3), 31.55 (d, $^3J(^{31}P\text{-}^{13}C)$ = 12.5 Hz, C5), 29.42 (C4), 28.63 (d, $^1J(^{31}P\text{-}^{13}C)$ = 12.3 Hz, C7), 25.51 (d, $^2J(^{31}P\text{-}^{13}C)$ = 16.2 Hz, C6), 23.58 (C2), 15.62 (C1); **^{31}P{^{1}H} NMR** (C_6D_6, 202.3 MHz): δ (ppm) = −16.38 (s).

*Tris(11-diphenylphosphinoundecyl)ethoxysilane **6***

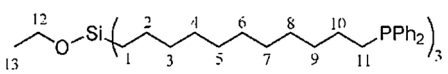

The ethoxysilane **3** (375 mg, 0.703 mmol), AIBN (104 mg, 0.634 mmol) and Ph_2PH (575 mg, 3.040 mmol) are combined in a Schlenk flask, heated to 70 °C and stirred for 4 d. The conversion is monitored by ^{31}P NMR of the reaction mixture. After the reaction is complete, the crude product is purified by column chromatography (SiO_2, toluene) to give **6** (350 mg, 0.320 mmol) as a colorless viscous oil in 45% yield.

^{1}H NMR ($CDCl_3$, 499.7 MHz): δ (ppm) = 7.39–7.44 (m, 12H, H_o), 7.30–7.35 (m, 18H, H_m, H_p), 3.65 (q, $^3J(^1H\text{-}^1H)$ = 6.9 Hz, 2H, H12), 2.01–2.06 (m, 6H, H11), 1.37–1.48 (m, 12H, overlapping H2, H10), 1.20–1.35 (m, 42H, overlapping H3-H9), 1.17 (t, $^3J(^1H\text{-}^1H)$ = 6.9 Hz, 3H, H13), 0.55-0.61 (m, 6H, H1); **^{13}C{^{1}H} NMR** ($CDCl_3$, 125.7 MHz): δ (ppm) = 139.05 (d, $^1J(^{31}P\text{-}^{13}C)$ = 13.0 Hz, C_i), 132.67 (d, $^2J(^{31}P\text{-}^{13}C)$ = 18.3 Hz, C_o), 128.38 (C_p), 128.32 (d, $^3J(^{31}P\text{-}^{13}C)$ = 6.5 Hz, C_m), 58.35 (C12), 33.70 (C3), 31.23 (d, $^1J(^{31}P\text{-}^{13}C)$ = 12.9 Hz, C11), 29.66 (C4*), 29.59 (C5*), 29.52 (C6*), 29.31 (C7*), 29.28 (C8*), 28.04 (d, $^3J(^{31}P\text{-}^{13}C)$ = 11.0 Hz, C9), 25.96 (d, $^2J(^{31}P\text{-}^{13}C)$ = 15.9 Hz, C10), 23.19 (C2), 18.67 (C13), 13.66 (C1), *assignments interchangeable; **^{31}P{^{1}H} NMR** ($CDCl_3$, 202.3 MHz): δ (ppm) = −16.33 (s); **^{29}Si{^{1}H} NMR** ($CDCl_3$, 79.4 MHz): δ (ppm) = 15.53 (s).

*Hexakis(11-diphenylphosphinoundecyl)disiloxane **6d***

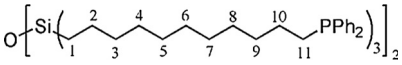

The disiloxane **3b** (628 mg, 0.633 mmol), AIBN (140 mg, 0.853 mmol) and Ph_2PH (1.151 g, 6.086 mmol) are combined in a Schlenk flask, heated to 70 °C and stirred for 4 d. When complete conversion is reached, as monitored by ^{31}P NMR of the reaction mixture, the crude product is purified by column chromatography (SiO_2, toluene) to give **6** (950 mg, 0.450 mmol) as a colorless viscous oil in 71% yield.

^{1}H NMR ($CDCl_3$, 499.7 MHz): δ (ppm) = 7.44–7.52 (m, 24H, H_o), 7.28–7.41 (m, 36H, H_m, H_p), 2.06–2.14 (m, 12H, H11), 1.26–1.58 (m, 108H, overlapping H2-H10), 0.61-0.69 (m, 12H, H1); **^{13}C{^{1}H} NMR** ($CDCl_3$, 125.7 MHz): δ (ppm) = 139.03 (d, $^1J(^{31}P\text{-}^{13}C)$ = 13.3 Hz, C_i), 132.65 (d, $^2J(^{31}P\text{-}^{13}C)$ = 17.9 Hz, C_o), 128.29 (d, $^3J(^{31}P\text{-}^{13}C)$ = 7.9 Hz, C_m), 128.17 (C_p), 33.59 (C3), 31.19 (d, $^1J(^{31}P\text{-}^{13}C)$ = 12.2 Hz, C11), 29.61 (C4*), 29.53 (C5*), 29.48 (C6*), 29.31 (C7*), 29.25 (C8*), 28.02 (d, $^3J(^{31}P\text{-}^{13}C)$ = 11.6 Hz, C9), 25.94 (d, $^2J(^{31}P\text{-}^{13}C)$ = 14.8 Hz, C10), 23.07 (C2), 15.06 (C1), *assignments interchangeable; **^{31}P{^{1}H} NMR** ($CDCl_3$, 202.3 MHz): δ (ppm) = −16.34 (s).

*Rhodium complex **15***

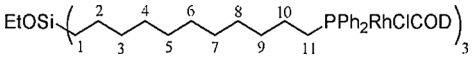

RhClpyCOD (35 mg, 0.107 mmol) is dissolved in 10 ml of CH_2Cl_2. Ligand **6** (39 mg, 0.036 mmol), dissolved in CH_2Cl_2 (15 ml), is added dropwise and the reaction mixture is stirred at RT for 4 h. Then the solvent is removed *in vacuo* and the residue washed with copious amounts of pentane. After drying the residue *in vacuo* **11** (50 mg, 0.021 mmol) is obtained as an orange powder in 60% yield.

^{1}H NMR ($CDCl_3$, 499.7 MHz): δ (ppm) = 7.59–7.65 (m, 12H, H_o), 7.34–7.41 (m, 18H, H_m, H_p), 5.46 (s, 6H, COD-H_{Olefin}), 3.65 (q, $^3J(^1H\text{-}^1H)$ = 6.9 Hz, 2H, CH_2O), 2.99 (s, 6H, COD-H_{Olefin}), 2.43–2.50 (m, 6H, H11), 2.23–2.41 (m, 12H, COD-H_{alkyl}), 1.96–2.05 (m, 6H, H11), 1.76–1.89 (m, 12H, COD-H_{alkyl}), 1.37–1.45 (m, 6H, H10), 1.19–1.33 (m, 48H, H2-H9), 1.15 (t, $^3J(^1H\text{-}^1H)$ = 6.9 Hz, 3H, CH_3), 0.52-0.59 (m, 6H, H1); **^{13}C{^{1}H} NMR** ($CDCl_3$, 125.7 MHz): δ (ppm) = 133.51 (d, $^2J(^{31}P\text{-}^{13}C)$ = 12.2 Hz, C_o), 132.35 (d, $^1J(^{31}P\text{-}^{13}C)$ = 39.5 Hz, C_i), 129.88 (d, $^4J(^{31}P\text{-}^{13}C)$ = 2.1 Hz, C_p), 128.08 (d, $^3J(^{31}P\text{-}^{13}C)$ = 9.4 Hz, C_m), 104.35 (dd, $^1J(^{103}Rh\text{-}^{13}C)$ = 12.6 Hz, $^2J(^{31}P\text{-}^{13}C)$ = 6.4 Hz, COD-C_{olefin}), 70.10 (d, $^1J(^{103}Rh\text{-}^{13}C)$ = 6.8 Hz, COD-C_{olefin}), 58.29 (CH_2O), 33.68 (C3), 32.91 (d, $^3J(^{31}P\text{-}^{13}C)$ = 2.3 Hz, C9), 31.44 (d, $^2J(^{31}P\text{-}^{13}C)$ = 13.5 Hz, C10), 29.58 (C4*, overlapping with COD-C_{alkyl}), 29.56 (d, $^1J(^{31}P\text{-}^{13}C)$ = 8.0 Hz, C11), 29.29 (C5*), 29.14 (C6*), 28.68 (COD-C_{alkyl}), 27.96 (C7*), 25.98 (C8*), 23.16 (C2), 18.63 (CH_3), 13.63 (C1), *interchangeable assignments; **^{31}P{^{1}H} NMR** ($CDCl_3$, 202.3 MHz): δ (ppm) = 26.14 (d, $^1J(^{103}Rh\text{-}^{31}P)$ = 147.9 Hz).

Author contributions

The manuscript was written through contributions of all authors. All authors have given approval of the final version of the manuscript.

Declaration of Competing Interest

The authors declare no competing financial interest.

Acknowledgements

This material is based upon work supported by the National Science Foundation under the Grant Numbers CHE-1300208 and CHE-1900100, and by the Welch Foundation (A-1706). The FE-SEM acquisition was supported by the National Science Foundation under DBI-0116835, and we thank Dr. H. Kim of the Microscopy and Imaging Center (MIC) of Texas A&M University for the measurements. We thank Prof. Dr. G. Helmchen for a sample of DBCOT, and Jordon W. Benzie for a literature check.

Appendix A. Supplementary data

Supplementary material related to this article can be found, in the online version, at doi:https://doi.org/10.1016/j.mcat.2019.110629.

References

[1] J.A. Gladysz, Pure Appl. Chem. 73 (2001) 1319–1324.
[2] (a) J.A. Gladysz, D.P. Curran, I.T. Horvath, Handbook of Fluorous Chemistry, Wiley-VCH Verlag GmbH & Co, KGaA, 2004;
(b) J.J.J. Juliette, D. Rutherford, I.T. Horváth, J.A. Gladysz, J. Am. Chem. Soc. 121 (1999) 2696–2704;
(c) M.-A. Guillevic, C. Rocaboy, A.M. Arif, I.T. Horváth, J.A. Gladysz, Organometallics 17 (1998) 707–717;
(d) J.J.J. Juliette, J.A. Gladysz, I.T. Horváth, Angew. Chem. Int. Ed. 36 (1997) 1610–1612.
[3] L.V. Dinh, J.A. Gladysz, Angew. Chem. Int. Ed. 44 (2005) 4095–4097.
[4] (a) P. Barbaro, F. Liguori (Eds.), Heterogenized Homogeneous Catalysts for Fine Chemicals Production, Springer, Heidelberg, 2010;
(b) F.R. Hartley, Supported Metal Complexes, Reidel, D. Publ. Co., Dordrecht, The Netherlands, 1985;
(c) D.E. DeVos, I.F.J. Vankelecom, P.A. Jacobs (Eds.), Chiral Catalyst Immobilization and Recycling, Wiley-VCH, Weinheim, 2000;
(d) G. Rothenberg, Catalysis: Concepts and Green Applications, Wiley-VCH, Weinheim, 2008.
[5] J. Blümel, Coord. Chem. Rev. 252 (2008) 2410–2423.
[6] C. Merckle, J. Blümel, Chem. Mater. 13 (2001) 3617–3623.
[7] K.D. Behringer, J. Blümel, Inorg. Chem. 35 (1996) 1814–1819.
[8] R. Fetouaki, A. Seifert, M. Bogza, T. Oeser, J. Blümel, Inorg. Chim. Acta 359 (2006) 4865–4873.
[9] (a) M. Bogza, T. Oeser, J. Blümel, J. Organomet. Chem. 690 (2005) 3383–3389;
(b) N. Masciocchi, S. Galli, M. Bogza, J. Blümel, Powder Diffr. 22 (2007) 55–58.
[10] G. Tsiavaliaris, S. Haubrich, C. Merckle, J. Blümel, Synlett (2001) 391–393.
[11] F. Piestert, R. Fetouaki, M. Bogza, T. Oeser, J. Blümel, Chem. Commun. (2005) 1481–1483.
[12] (a) J. Blümel, J. Am. Chem. Soc. 117 (1995) 2112–2113;
(b) K.D. Behringer, J. Blümel, J. Liq, Chromatogr. 19 (1996) 2753–2765.
[13] K.D. Behringer, J. Blümel, Chem. Commun. (1996) 653–654.
[14] R. Silbernagel, A. Díaz, E. Steffensmeier, A. Clearfield, J. Blümel, J. Mol. Catal. A 394 (2014) 217–223.
[15] Merck silica 40, average particle size 0.063-0.2 mm, specific surface area 750 m^2/g, average pore diameter 40 Å.
[16] (a) E.F. Vansant, P. VanDer Voort, K.C. Vrancken, Characterization and Chemical Modification of the Silica Surface, Elsevier, Amsterdam, 1995;
(b) R.P.W. Scott, Silica Gel and Bonded Phases, John Wiley and Sons, New York, 1993.
[17] (a) S. Reinhard, P. Soba, F. Rominger, J. Blümel, Adv. Synth. Catal. 345 (2003) 589–602.
[18] S. Reinhard, K.D. Behringer, J. Blümel, New J. Chem. 27 (2003) 776–778.
[19] K.J. Cluff, N. Bhuvanesh, J. Blümel, Chem. Eur. J. 21 (2015) 10138–10148.
[20] J.C. Pope, T. Posset, N. Bhuvanesh, J. Blümel, Organometallics 33 (2014) 6750–6753.
[21] T. Posset, J. Blümel, J. Am. Chem. Soc. 128 (2006) 8394–8395.
[22] T. Posset, J. Guenther, J. Pope, T. Oeser, J. Blümel, Chem. Commun. 47 (2011) 2059–2061.
[23] J. Guenther, J. Reibenspies, J. Blümel, Adv. Synth. Catal. 353 (2011) 443–460.
[24] (a) C. Merckle, J. Blümel, Adv. Synth. Catal. 345 (2003) 584–588;
(b) C. Merckle, J. Blümel, Top. Catal. 34 (2005) 5–15.
[25] C. Merckle, S. Haubrich, J. Blümel, J. Organomet. Chem. 627 (2001) 44–54.
[26] (a) B. Beele, Dissertation 2010, Heidelberg.
(b) J.A. Osborn, F.H. Jardine, J.F. Young, G. Wilkinson, J. Chem. Soc. A (1966) 1711–1732
[27] T. Posset, F. Rominger, J. Blümel, Chem. Mater. 17 (2005) 586–595.
[28] (a) J. Blümel, Inorg. Chem. 33 (1994) 5050–5056;
(b) J. Sommer, Y. Yang, D. Rambow, J. Blümel, Inorg. Chem. 43 (2004) 7561–7563.
[29] Y. Yang, B. Beele, J. Blümel, J. Am. Chem. Soc. 130 (2008) 3771–3773.
[30] B. Beele, J. Guenther, M. Perera, M. Stach, T. Oeser, J. Blümel, New J. Chem. 34 (2010) 2729–2731.
[31] J.H. Baker, N. Bhuvanesh, J. Blümel, J. Organomet. Chem. 847 (2017) 193–203.
[32] (a) T.M. Duncan, A Compilation of Chemical Shift Anisotropies, Farragut Press, Chicago, IL, 1990;
(b) C.A. Fyfe, Solid-State NMR for Chemists, C.F.C. Press, Guelph, Canada, 1983;
(c) M.J. Duer, Introduction to Solid-State NMR Spectroscopy, Blackwell Publishing, Oxford, 2004.
[33] S. Reinhard, J. Blümel, Magn. Reson. Chem. 41 (2003) 406.
[34] S. Brenna, T. Posset, J. Furrer, J. Blümel, Chem. Eur. J. 12 (2006) 2880–2888.
[35] (a) 1st ed., J.G. de Vries, C.J. Elsevier (Eds.), The Handbook of Homogeneous Hydrogenation, Vols 1-3 Wiley-VCH, Weinheim, 2007;
Adv. Synth. Catal. 2003, 345, vols. 1 + 2, Special Issue on Hydrogenation, including, e.g.: W. S. Knowles, Adv. Synth. Catal. 2003, 345, 3; R. Noyori, Adv. Synth. Catal. 2003, 345, 15; T. Imamoto, Adv. Synth. Catal. 2003, 345, 79.
(b) G. Ertl, H. Knözinger, F. Schüth, J. Weitkamp (Eds.), Handbook of Heterogeneous Catalysis, 2nd ed., Wiley-VCH, Weinheim, 2008;
(c) M. Wende, R. Meier, J.A. Gladysz, J. Am. Chem. Soc. 123 (2001) 11490 and lit. cited therein;
(e) D.M. Heinekey, A. Lledós, J.M. Lluch, Chem. Soc. Rev. 33 (2004) 175–182
[36] (a) D. Rutherford, J.J.J. Juliette, C. Rocaboy, I.T. Horváth, J.A. Gladysz, Catal. Today 42 (1998) 381–388;
(b) K. Kromm, B.D. Zwick, O. Meyer, F. Hampel, J.A. Gladysz, Chemistry 7 (2001) 2015–2027;
(c) K. Kromm, P.L. Osburn, J.A. Gladysz, Organometallics 21 (2002) 4275–4280;
(d) T. Soós, B.L. Bennett, D. Rutherford, L.P. Barthel-Rosa, J.A. Gladysz, Organometallics 20 (2001) 3079–3086;
(e) C. Emnet, K.M. Weber, J.A. Vidal, C.S. Consorti, A.M. Stuart, J.A. Gladysz, Adv. Synth. Catal. 348 (2006) 1625–1634;
(f) D. Mandal, M. Jurisch, C.S. Consorti, J.A. Gladysz, Chem. Asian J. 3 (2008) 1772–1782.
[37] M. Perera, Master's Thesis, Texas A&M University, 2011.
[38] M. Baacke, O. Stelzer, V. Wray, Chem. Ber. 113 (1980) 1356–1369.
[39] (a) S.H. Ahn, K.J. Cluff, N. Bhuvanesh, J. Blümel, Angew. Chem. Int. Ed. 54 (2015) 13341–13345;
(b) S.H. Ahn, N. Bhuvanesh, J. Blümel, Chem. Eur. J. 23 (2017) 16998–17009;
(c) S.H. Ahn, N. Bhuvanesh, J. Blümel, ACS Sustainable Chem. Eng. 6 (2018) 6829–6840;
(d) F.F. Arp, N. Bhuvanesh, J. Blümel, Dalton Trans. (2019), https://doi.org/10.1039/C9DT03070K;
(e) C.R. Hilliard, N. Bhuvanesh, J.A. Gladysz, J. Blümel, Dalton Trans. 41 (2012) 1742–1754;
(f) C.R. Hilliard, S. Kharel, K.J. Cluff, N. Bhuvanesh, J.A. Gladysz, J. Blümel, Chem. Eur. J. 20 (2014) 17292–17295;
(g) S. Kharel, N. Bhuvanesh, J.A. Gladysz, J. Blümel, Chem. Asian J. 14 (2019) 2704–2711.
[40] (a) E.Y. Tupikina, M. Bodensteiner, P.M. Tolstoy, G.S. Denisov, I.G. Shenderovich, J. Phys. Chem. C 122 (2018) 1711–1720;
(b) G. Begimova, E.Y. Tupikina, V.K. Yu, G.S. Denisov, M. Bodensteiner, I.G. Shenderovich, J. Phys. Chem. C 120 (2016) 8717–8729;
(c) N.A. Bewick, A. Arendt, Y. Li, S. Szafert, T. Lis, K.A. Wheeler, J. Young, R. Dembinski, Curr. Org. Chem. 19 (2015) 469–474.
[41] (a) K.J. Cluff, J. Blümel, Organometallics 35 (2016) 3939–3948;
(b) K.J. Cluff, J. Blümel, Chem. Eur. J. 22 (2016) 16562–16575;
(c) K.J. Cluff, J. Blümel, Organometallics 33 (2014) 2671–2680;
(d) K.J. Cluff, M. Schnellbach, C.R. Hilliard, J. Blümel, J. Organomet. Chem. 744 (2013) 119–124.
[42] D. Brodzki, G. Pannetier, J. Organomet. Chem. 63 (1973) 431–440.
[43] CCDC 894281 contains the supplementary crystallographic data of ClRhpyCOD for this paper. These data can be obtained free of charge from the Cambridge Crystallographic Data Centre via www.ccdc.cam.ac.uk/data_request/cif. $C_{13}H_{17}ClNRh$ (M = 325.63 g/mol), brown plate, 0.32× 0.22× 0.13 mm^3, monoclinic, space group $P2_1/c$ (No. 14), a = 17.177(5) Å, b = 11.143(3) Å, c = 13.994(4) Å, β = 113.714(4)°, V = 2452.2(12) $Å^3$, Z = 8, T = 150.15 K, μ(MoKα) = 1.581 mm^{-1}, D_{calc} = 1.764 g/cm^3, 42195 reflections measured (3.178° ≤ 2Θ 55.22°), 5659 unique (R_{int} = 0.0307, R_σ = 0.0184) which were used in all calculations. The final R_1 was 0.0291 (I > 2σ(I)) and wR_2 was 0.0716 (all data).
[44] J. Rajput, A.T. Hutton, J.R. Moss, H. Su, C. Imrie, J. Organomet. Chem. 691 (2006) 4573–4588.
[45] (a) S. Kharel, N. Bhuvanesh, J.A. Gladysz, J. Blümel, Inorg. Chim. Acta 490 (2019) 215–219;

(b) Y.R. Jorapur, T. Shimada, Synlett 23 (2012) 1633–1638.
[46] V.V.S. Reddy, A. Varshney, G.M. Gray, J. Organomet. Chem. 391 (1990) 259–266.
[47] J.A. Widegren, R.G. Finke, J. Mol. Catal. A Chem. 198 (2003) 317–341.
[48] C. Elschenbroich, Organometallics, 3rd ed., Wiley-VCH: Weinheim, Germany, 2006.
[49] J.P. Collman, K.M. Kosydar, M. Bressan, W. Lamanna, T. Garret, J. Am. Chem. Soc. 106 (1984) 2569-2519.
[50] D.R. Anton, R.H. Crabtree, Organometallics 2 (1983) 855–859.
[51] H. Beyer, K. Chatziapostolou, K. Köhler, Top. Catal. 52 (2009) 1752–1756.
[52] O.V. Dolomanov, L.J. Bourhis, R.J. Gildea, J.A.K. Howard, H. Puschmann, J. Appl. Cryst. 42 (2009) 339–341.
[53] G.M. Sheldrick, Acta Cryst. A 71 (2015) 3–8.
[54] G.M. Sheldrick, Acta Cryst. A 64 (2008) 112–122.